Journal of Hydrology: Regional Studies 44 (2022) 101212

Contents lists available at ScienceDirect

Journal of Hydrology: Regional Studies

journal homepage: www.elsevier.com/locate/ejrh

Assessment of spatial and temporal variability of groundwater level in the aquifer system on the flanks of Mount Meru, Northern Tanzania

George Bennett [a,b,*], Marc Van Camp [a], Ceven Shemsanga [c], Matthieu Kervyn [d], Kristine Walraevens [a]

[a] *Laboratory for Applied Geology and Hydrogeology, Department of Geology, Ghent University, Belgium*
[b] *Department of Mining and Mineral Processing Engineering, University of Dodoma, Tanzania*
[c] *Department of Geology, University of Dodoma, Tanzania*
[d] *Physical Geography, Department of Geography, Vrije Universiteit Brussel, Belgium*

ARTICLE INFO

Keywords:
Groundwater level assessment
Spatial-temporal variability
Piezometric map
Groundwater level fluctuation
Mount Meru
Tanzania

ABSTRACT

Study region: Mount Meru located in Northern Tanzania.
Study focus: Groundwater level monitoring is essential for uncovering the spatial-temporal variation of groundwater levels in a studied aquifer, helping discussions on the sustainable use and management of groundwater resources. This study analyses the spatial and temporal variability of groundwater level in the shallow aquifer system on the flanks of Mount Meru. Time series analysis of groundwater level measurements obtained in two hydrologic years: 2018–2019 and 2019–2020 is applied.
New hydrological insights for the region: On the north-eastern flank of Mount Meru, at Ngarenanyuki, there is a rise of about 1.80 m between the static water levels in April 2018 and December 2020 in the shallow aquifer, whereas on the western flank, at Mamsa, there is a decrease of about 0.50 m between the static water levels in May 2018 and December 2020 in the shallow aquifer, this can be attributed to low/reduced recharge (due to very low hydraulic conductivity and semi-confined condition of the aquifer), or exploitation. Hence, the current pumping practices in the aquifer on the western flank should be restrained for sustainable groundwater management.

1. Introduction

Groundwater level monitoring is essential for uncovering the spatial-temporal variation of groundwater levels in a studied aquifer, helping discussions on the sustainable use and management of groundwater resources. The spatial-temporal variation of groundwater levels in the aquifer is influenced by a variety of factors such as climate, hydrology, geology and human activities (Cui et al., 2020; Marques et al., 2020; Kong et al., 2022). The different hydrologic factors which can simultaneously play an important role in groundwater level fluctuations can be grouped into two groups: natural and anthropogenic. The natural factors include precipitation, evapotranspiration, atmospheric pressure fluctuations, tides and earthquakes, whereas the anthropogenic factors include pumping and

* Corresponding author at: Laboratory for Applied Geology and Hydrogeology, Department of Geology, Ghent University, Belgium.
E-mail address: george.bennett@udom.ac.tz (G. Bennett).

https://doi.org/10.1016/j.ejrh.2022.101212
Received 14 April 2022; Received in revised form 27 August 2022; Accepted 13 September 2022
2214-5818/

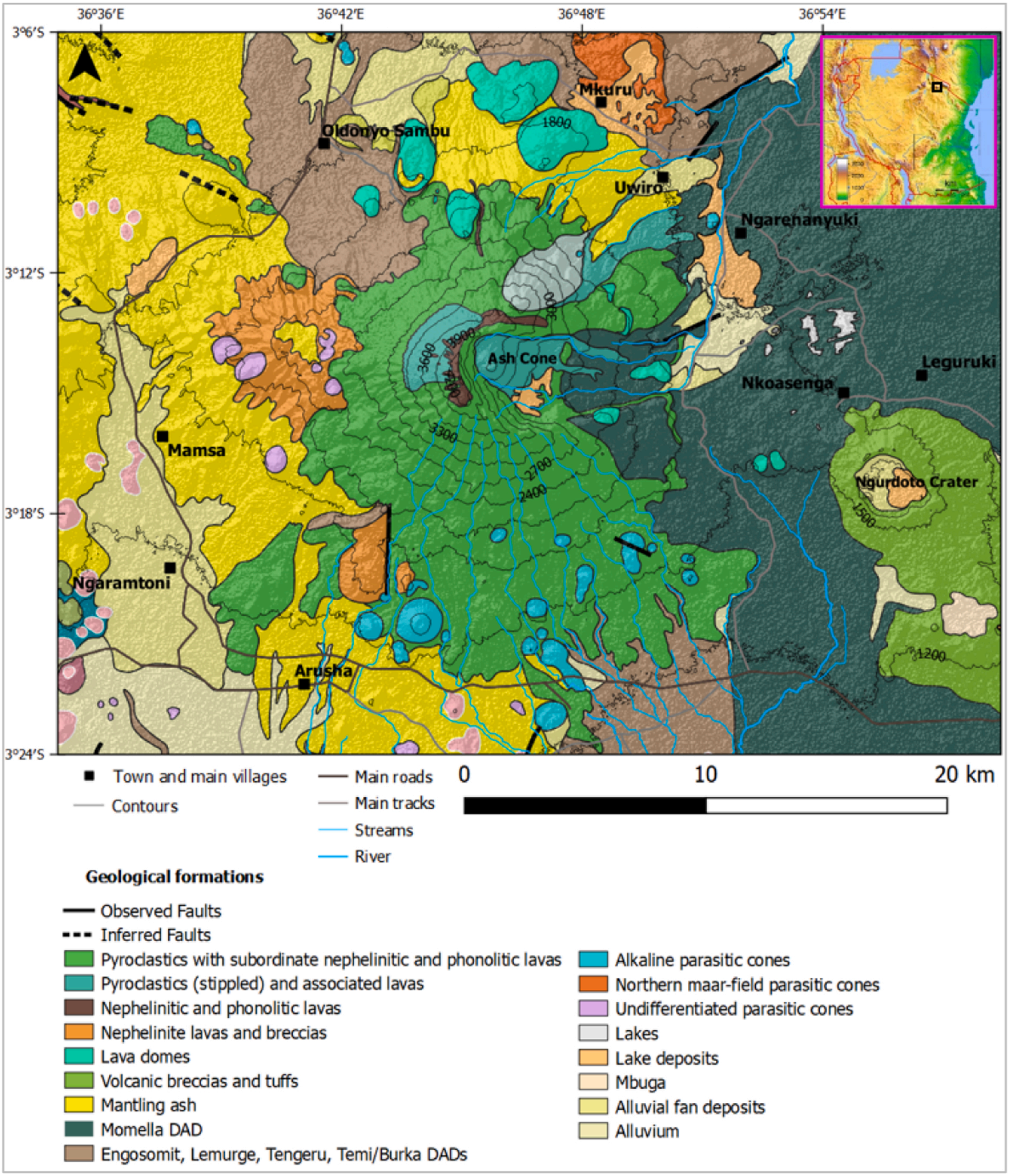

Fig. 1. The inserted small map of Tanzania was modified after Mapsland (2021), the original image is under Creative Commons Attribution-ShareAlike 3.0 Unported (CC BY-SA 3.0) license.
(a) Geological map of the study area adapted from Bennett et al. (2021), indicating different geological formations. (b) A small map inserted in the top right corner is the map of Tanzania adapted from Bennett et al. (2022a), showing the location of Mount Meru using a black lined square.

drainage (Healy and Cook, 2002; Maréchal et al., 2002; Singaraja et al., 2018; Lee et al., 2020; Shibata et al., 2020). The groundwater level fluctuations can either be short-term or long-term. The short-term fluctuations can be due to response to rainfall, pumping and barometric pressure variations, whereas the long-term can be due to naturally occurring changes in climate and changes due to anthropogenic activities (such as pumpage, irrigation, induced infiltration, and changes in land usage) (Healy and Cook, 2002).

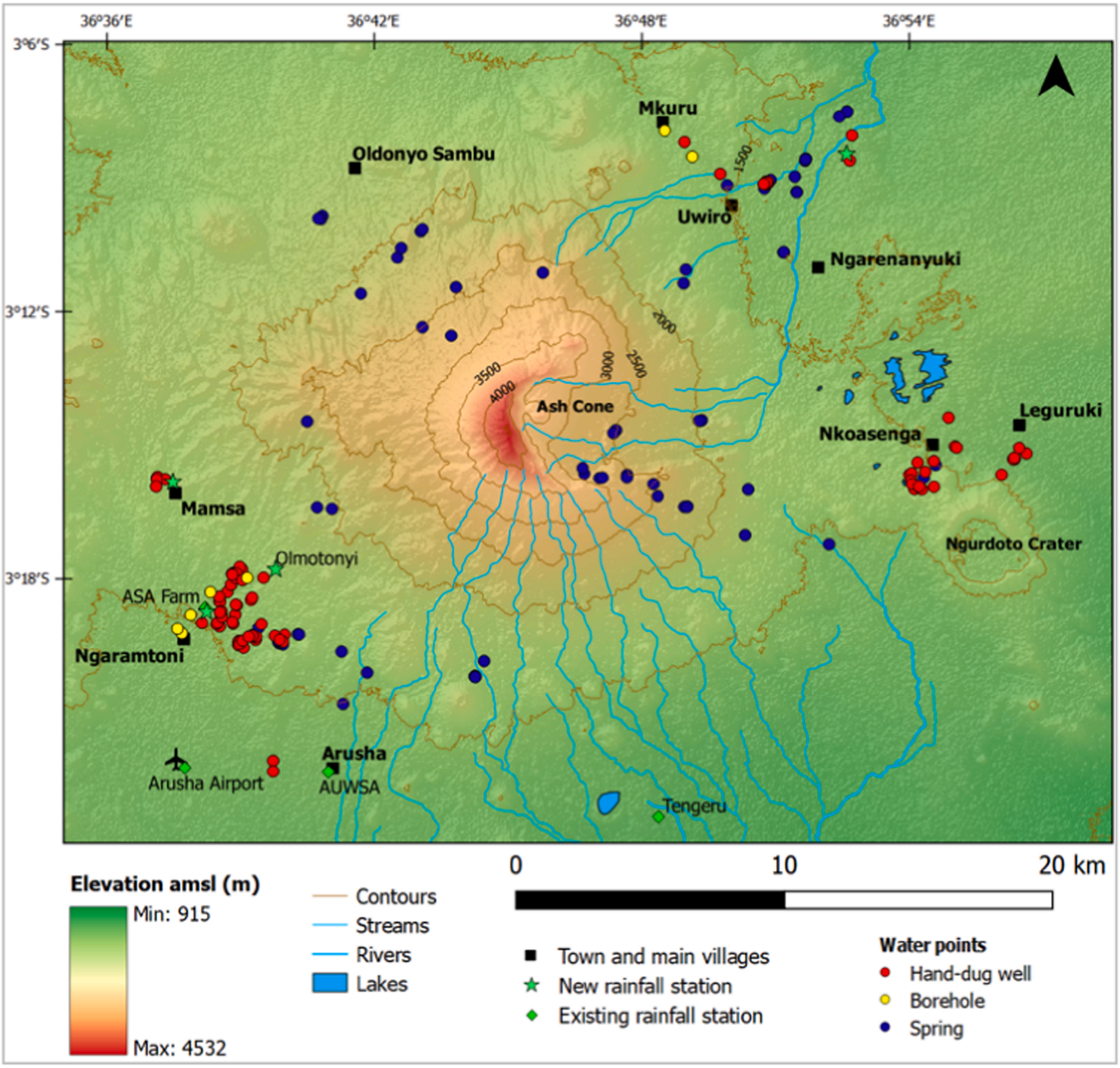

Fig. 2. A map showing the Digital Elevation Model (DEM) of the study area and the spatial distribution of hand-dug wells, boreholes, springs, and rainfall stations used for investigating the groundwater-level response to rainfall.

Seasonal fluctuations are observed in the long-term groundwater level fluctuations, this is due to the seasonality of evapotranspiration, precipitation, and irrigation (Healy and Cook, 2002). Since precipitation is the primary source of groundwater recharge, thus the temporal and spatial distribution of precipitation determines the spatial-temporal variation of the groundwater level in the aquifer.

To the best of our knowledge, no study has been reported on the groundwater level monitoring in the aquifer system around Mount Meru for investigation of the groundwater-level response to rainfall. Therefore, the present research investigates the spatial-temporal groundwater level response to rainfall in the shallow aquifer system on the eastern, northern, western, and south-western flanks of Mount Meru.

2. Materials and methods

2.1. Study area

2.1.1. Location, topography, and climate

The study area covers most of the slopes of Mount Meru in Arusha region, northern Tanzania, and occupies about 1000 km^2 (Fig. 1) (Bennett et al., 2021, 2022a). The topography of the study area is dominated by Mount Meru, with several parasitic cones in the vicinity (Bennett et al., 2021, 2022a). The study area experiences a bimodal rainfall pattern; the long "masika" rains extend from late February to late May and the short "vuli" rains from early November to early January. The dry "kiangazi" season is from June to October (Bennett et al., 2021, 2022a). The areas in the windward side of the mountain (eastern and southern flanks) experience a subtropical highland climate, whereas areas in the leeward side (the northern flank) experience a semi-arid climate (Bennett et al., 2021, 2022a). The average annual rainfall on the north-eastern, western, south-western and southern flank is 638, 905, 958 and 962 mm respectively (Bennett et al., 2021, 2022a).

2.1.2. Geological and hydrogeological setting

The geology of the study area, and the link between the local geology and hydrogeology in the area has been described in Bennett et al. (2021). The aquifer system on the flanks of Mount Meru is a sloping aquifer with sloping beds. On the far east of the eastern flank (i.e., on the northern flank of Ngurdoto crater), the aquifer is composed of debris avalanche deposits, while on the north-eastern and west flanks the aquifer is composed of weathered fractured lava, whereas on the south-western flank, the aquifer is composed of different layers: pyroclastics on the top, weathered fractured lava, weathered pyroclastics, and weathered fractured lava at the bottom. The aquifer is semi-confined on the north-eastern and western flanks; on the north-eastern flank, the overlying debris avalanche deposits acting as an aquitard, while on the western flank, the overlying layers: pyroclastics and unweathered lava acting as an aquitard and aquiclude, respectively. The aquifer is unconfined on the far east of the eastern flank and south-western flank (Bennett et al., 2022b). Mount Meru is an active stratovolcano located within the Northern Tanzanian Divergence Zone of the eastern branch of the East African Rift. The lithology in the study area is dominated by volcanic rocks – lava flows, pyroclastic and debris avalanche deposits from the Mount Meru, with some alluvium, alluvial fan and lake deposits found around the volcano base (Fig. 1) (Bennett et al., 2021).

2.2. Inventory of groundwater monitoring points

The inventory of groundwater points has been discussed in detail in Bennett et al. (2021), it was conducted during four field campaigns: July – September 2017, March – September 2018, February – August 2019 and April – December 2020. A total of 95 groundwater wells: 7 boreholes (depth range from 48 m to 150 m) and 88 hand-dug wells (depth range from 0.7 m to 50 m) were used for groundwater level mapping. Fig. 2 shows the spatial distribution of hand-dug wells, boreholes, springs, and rainfall stations used for this study. The distribution of wells is in four clusters located at: Ngaramtoni and near Arusha town (south-western flank), Mamsa (western flank), Mkuru, Uwiro and Ngarenanyuki (north-eastern flank) and, Nkoasenga and Leguruki (far east of the eastern flank). In this study, a well with depth greater than 50 m is considered as deep well, therefore, all hand-dug wells are classified as shallow wells whereas one borehole is classified as shallow well and the rest as deep wells. Shallow wells characterise the shallow aquifer whereas deep wells characterise the deep aquifer. From the 88 hand-dug wells, 74 % ($n = 65$) were used for groundwater level monitoring from 2018 to December 2020; 33 wells on the south-western flank, 19 on the far east of the eastern flank (i.e., on the northern flank of Ngurdoto crater), 9 on the north-eastern flank and 4 on the western flank. No borehole was monitored due to lack of frequent access. Therefore, this study reports the groundwater level fluctuations in the shallow aquifer system in the study area.

2.3. Groundwater level data collection and spring discharge measurements

From the 65 monitoring wells, high frequency automatic groundwater level measurements using divers and barodivers were conducted in seven wells. One well is on the western flank, at Mamsa, where diver and barodiver were installed on 04/05/2018. Another well is on the north-eastern flank, at Ngarenanyuki, where diver and barodiver were installed on 17/04/2018. Five wells are on the south-western flank, at Ngaramtoni; two wells, respectively, are installed with diver and barodiver, whereas the other three, respectively, are installed with diver only. The measurements in two wells are active since 22/10/2017, whereas in the other three wells are active since 04/05/2018, 23/09/2018 and 14/08/2019 respectively. Diver is used to monitor continuous record of water level and temperature fluctuations while barodiver measures atmospheric pressure and temperature. Divers/barodivers were programmed using Diver-Office 2017 from Van Essen Instruments, a computer software for programming and reading diver/barodiver. Additionally, manual groundwater level measurements were performed twice per month, sometimes once per month, by using a portable dip meter at 58 wells: 19 on the far east of the eastern flank (on the northern flank of Ngurdoto crater) (raw data are shown in Table 3 in the Appendix), 8 on the north-eastern flank (Table 4 in the Appendix), 3 on the western flank (Table 5 in the Appendix) and 28 on the south-western flank (Table 6 in the Appendix). Also, all automatic monitored wells were manually measured during the manual measurement campaigns, for data backup and verifying diver measurements. The locations of the wells were selected to ensure a good spatial coverage for the data acquisition in the study area. During manual water level measurements, it was not possible to conducts all the measurements before people fetching water for local consumption, consequently some measurements were dynamic groundwater level and not static groundwater level, this was identified as the major limitation. Only two wells were recorded for a short period, one went dry while the other became inaccessible.

For the extra 30 groundwater wells (raw data are shown in Table 7 in the Appendix), 26 were manually measured during field campaigns (15 were measured at least twice and at most fifth times, whereas 11 were measured once), data for two boreholes were obtained from Pangani Basin Water Board Arusha office (a government office), one borehole data were obtained from The Plaster House (a private organization in Arusha) and one borehole data were obtained from Ghiglieri et al. (2010).

Springs discharge monitoring was conducted on three flanks: north-eastern, north-western, and south-western flanks. On the north-eastern flank, two springs: S12 and S13 were monitored during the year 2019, and the measurements were done using pygmy current

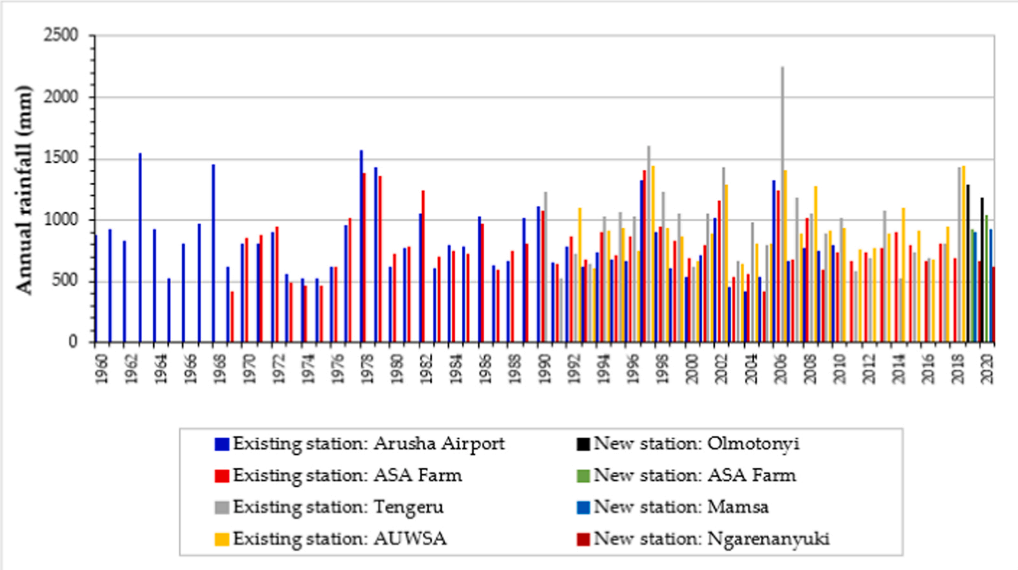

Fig. 3. Annual rainfall trend for the existing and new rainfall stations in the study area.

meter and float methods. On the north-western flank, two springs: S3 and S5 were monitored during the year 2019. The measurements in spring S3 were done using bucket and stopwatch method, whereas in spring S5 were done using both pygmy current meter and float methods. On the south-western flank, three springs: S21, S22 and S24 were monitored during the years 2018–2019, and the measurements were done using bucket and stopwatch method.

2.4. Rainfall data collection

In order to investigate the rainfall pattern in the study area, four automatic tipping bucket rain gauges (DAVIS rain gauge 6465 M (pole mounting version) connected with HOBO Pendant Event data logger) were installed in September 2018; one at Mamsa (western flank), one at Ngarenanyuki (north-eastern flank) and two at Ngaramtoni (south-western flank) (see Fig. 2) (Bennett et al., 2021). Also, rainfall data from existing rainfall stations within/near the study area (see Fig. 2) were acquired from four stations: Agricultural Seed Agency (ASA) Farm at Ngaramtoni with 50 years data (1969–2018), Arusha Airport with 51 years data (1960–2010), Arusha Urban Water Supply and Sanitation Authority (AUWSA) with 27 years data (1992–2018) and Tengeru Livestock Institute with 29 years data (1990–2018) (Bennett et al., 2021). Fig. 3 shows the annual rainfall trend for the existing and new rainfall stations in the study area.

2.5. Data processing and analysis

For the groundwater level data, before data analysis, the diver and barodiver data were visualised by using Diver-Office 2017 and then downloaded, whereas the manually measured data were visualised using Microsoft Excel 2019 by plotting arithmetic time-groundwater level depth graphs. Diver data were corrected for the barometric effect by using barodiver data to filter out water level fluctuations due to atmospheric pressure, to remain with the useful component that is due to aquifer storage changes. The barometric compensation was done manually by using Microsoft Excel 2019 by taking diver data minus barodiver data, for the data measured at same time. Also, the compensation was done automatically by using Diver-Office 2017 for comparison. The corrected data were changed to hydraulic head by subtracting them from topographic elevation data of the wells. Finally, the groundwater level contour map (piezometric map) was constructed using the hydraulic head data. For the large (regional) scale piezometric map, the hydraulic head was obtained by subtracting the average water depths in the study area from the Digital Elevation Model (DEM) of the area. The average water depths in the study area were obtained by interpolation of average water depths (under static water condition) at inventoried, and control points by using QGIS software. For the small (local) scale piezometric maps, the contour lines were freehand drawn by using the digitising tool in QGIS software, a geographic information system application that supports viewing, editing, and analysis of geospatial data.

For the rainfall data, before data analysis, data were visualised and downloaded by using HOBOware, a software package for visualising, graphing, analysis and downloading rainfall and temperature data from HOBO data loggers. Then, afterwards, data were analysed by using Microsoft Excel 2019. Furthermore, the rainfall data were used to create a rainfall map of the study by using interpolation technique in QGIS software. The inverse distance weighting (IDW) method was used for interpolation between the rainfall stations.

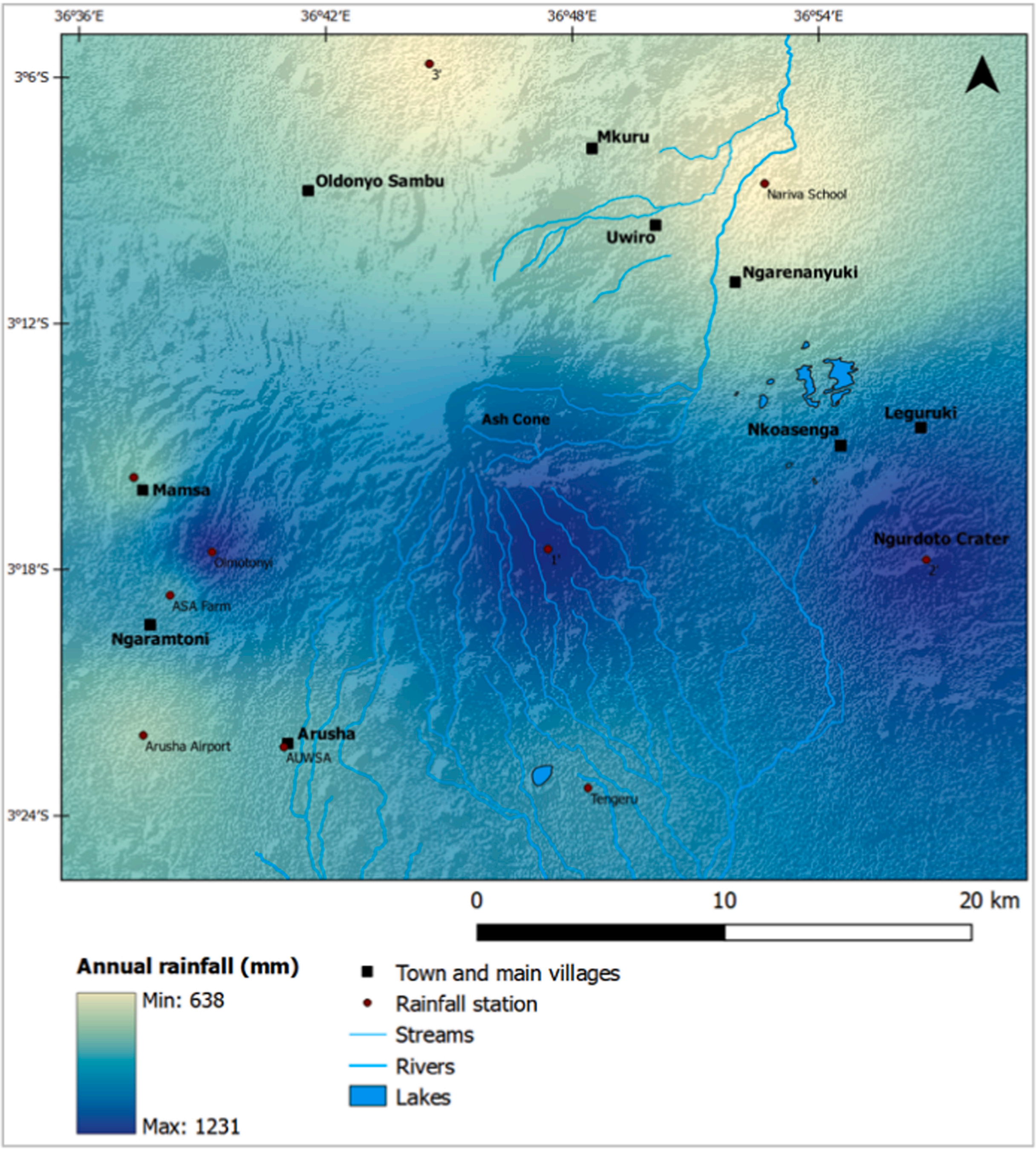

Fig. 4. Rainfall map showing spatial distribution of long-term average annual rainfall around Mount Meru.

3. Results and discussion

3.1. Spatial rainfall distribution

Fig. 4 shows the spatial distribution of long-term average annual rainfall around Mount Meru, the study area. The rainfall map was created by interpolation of the annual rainfall data at the existing and newly installed rainfall stations using the inverse distance weighting (IDW) method (Distance coefficient P = 2.00 was used).

The existing four stations; ASA Farm, Arusha Airport, AUWSA and Tengeru have average annual rainfall (in mm) of 800, 822, 942 and 981 respectively. The four newly installed rainfall stations: ASA Farm, Olmotonyi, Mamsa and Nariva school (at Ngarenanyuki)

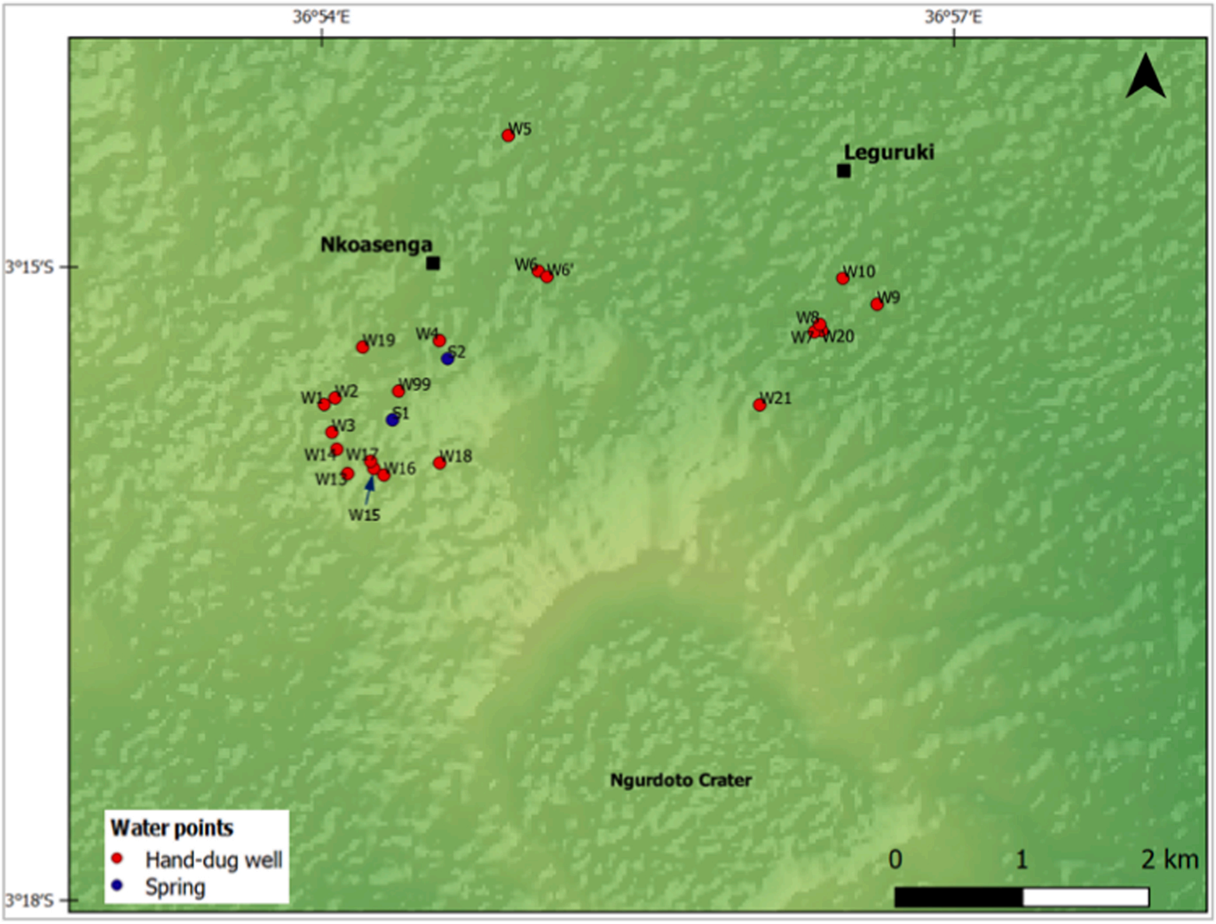

Fig. 5. A zoomed-in part of Fig. 2 showing the spatial distribution of hand-dug wells and springs on the northern flank of Ngurdoto crater used for investigating groundwater-level trends in the area.

have average annual rainfall (in mm) of 977, 1232, 905 and 638 respectively (Bennett et al., 2021). The newly installed automatic rain gauge at ASA Farm replaced the existing manual rain gauge. This was done due to the fact that, two stations were installed at Ngaramtoni: one at higher elevation (at Olmotonyi) and one at lower elevation (at ASA Farm, where was the only place of choice due to security) in order to analyse the spatial distribution of rainfall at different elevations. It should be mentioned that the rainfall data for the newly installed automatic rain gauge at ASA Farm shows a much higher value of the average annual rainfall (977 mm) than the average annual rainfall from the old data (800 mm); this is due to the fact that the value of 977 mm is for the 2 years data (2019–2020), which is a shorter period, whereas the value of 800 mm is for the 50 years data (1969–2018), which is a longer period. Due to a small number of stations and how they are distributed, most are clustered on the south-western flank, thus, three imaginary rainfall stations: 1′, 2′ and 3′ were added to generate a map which reflects a real field scenario. Stations 1′ and 2′ were assigned same value as Olmotonyi station, the areas roughly receive same amount of rainfall as they are located in the windward sides (eastern and southern flanks), while station 3′ was assigned same value as station at Nariva school, to cover a large area of the leeward sides (northern flank) which receives low rainfall (Bennett et al., 2021, 2022a). The area around Mount Meru receives orographic rainfall, hence high values of rainfall at high elevations in the windward sides are expected.

3.2. Spatial and temporal groundwater level variation, and groundwater flow

3.2.1. Far east of the eastern flank

Groundwater level monitoring was conducted in 15 hand-dug wells at Nkoasenga and 4 hand-dug wells at Leguruki. The shallow aquifer in these areas is composed of debris avalanche deposits. Fig. 5 (which is a zoomed-in part of Fig. 2) shows the spatial distribution of hand-dug wells and springs on the northern flank of Ngurdoto crater used for investigating groundwater-level trends on this flank. Fig. 6 shows hydraulic head fluctuations on this flank for the years 2018–2020. Some of the manual measurements are affected by water withdrawal from the wells; the "dips" in the time series data are due to the well not having reached static conditions (dynamic water levels), and these will not be considered in the analysis of fluctuations of static water level in the aquifer. Fig. 7 shows the conceptual groundwater flow model for this flank developed by Bennett et al. (2022a). The conceptual groundwater flow models

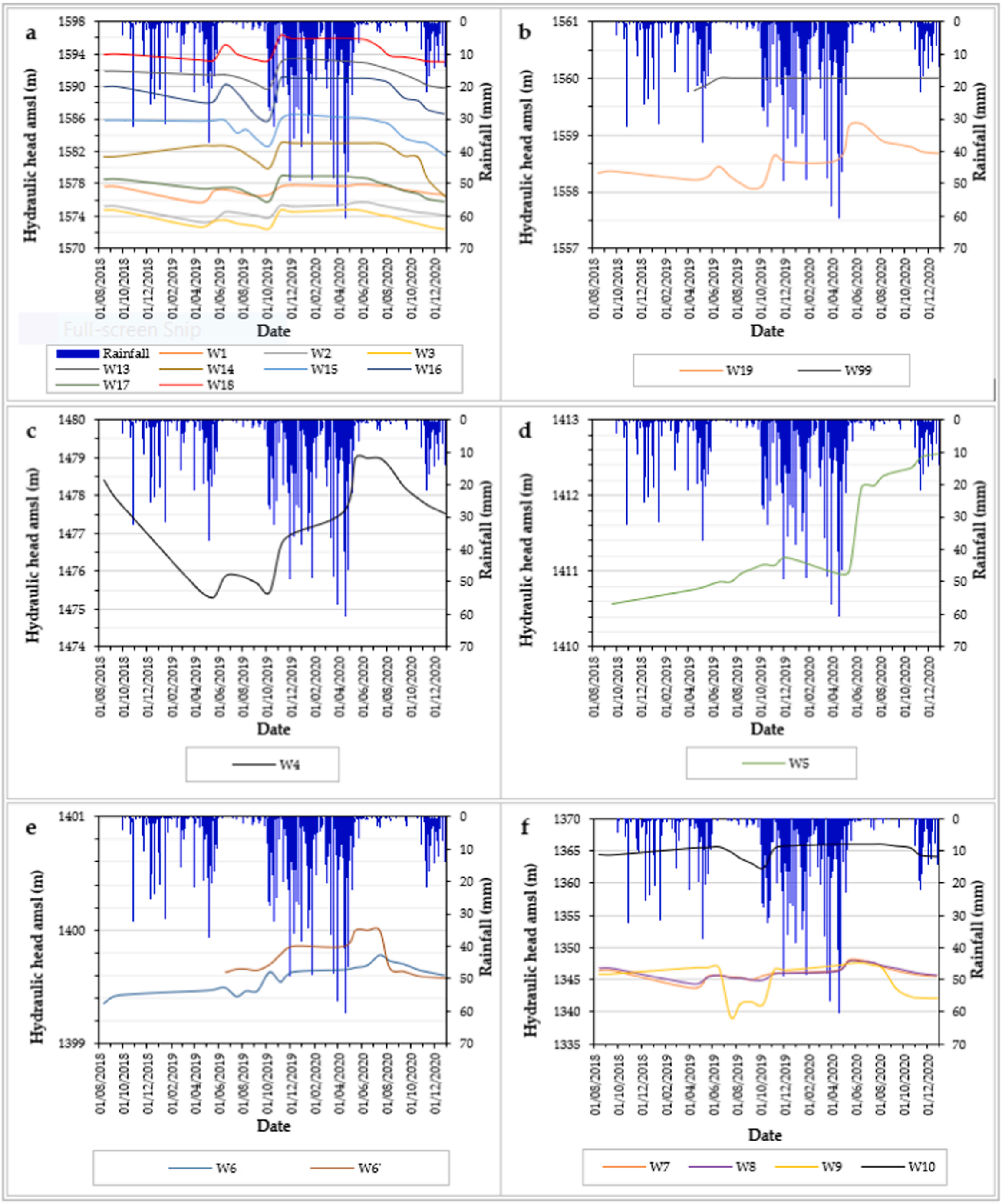

Fig. 6. Hydraulic head fluctuations at; (a to e) Nkoasenga and (f) Leguruki, and daily rainfall (Olmotonyi rainfall station) for the years 2018–2020.

for the different flanks in the study area were discussed in detail by Bennett et al., (2021, 2022a). Three different flow systems: local, intermediary, and regional were identified in the models. The models show the increase of groundwater mineralisation with water residence times (i.e., the increase of TDS along the flow path), and also indicate the influence of local flow system which lower groundwater mineralisation by mixing with intermediary and regional systems along the flow paths (Bennett et al., 2021, 2022a).

The hydrological year spans the period from 1 October to 30 September of the next year. The wells which are located close together show similar shape of the groundwater mound; such as W16 and W18 (the upper two lines) in Fig. 8a, W1, W2 and W3 (the lower three lines) in Fig. 8a, and the wells in Fig. 8b. The rainy season 2018–2019 was exceptionally dry. Recharge therefore took place mainly towards the end of the rainy season and was noticeable on most wells only after. W16 and W18 show clear recharge wave in June 2019,

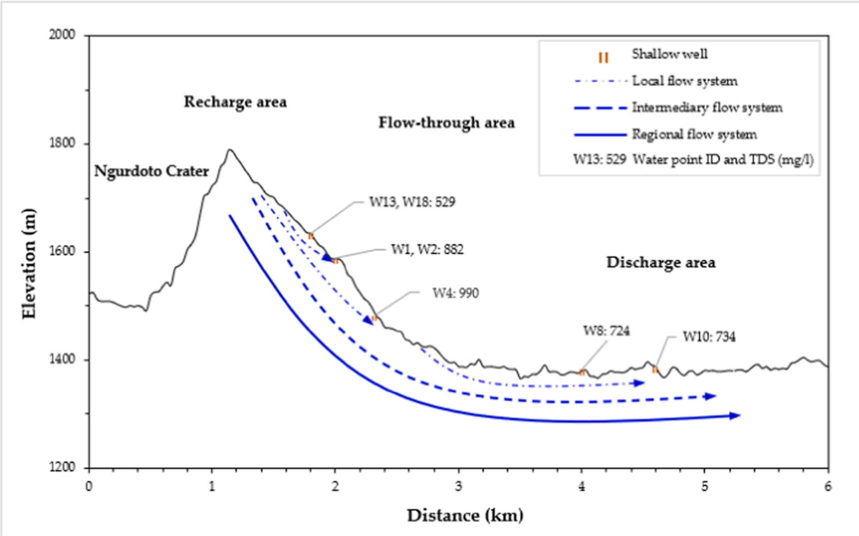

Fig. 7. Simplified groundwater flow conceptual model for the northern flank of Ngurdoto crater, showing the increase of groundwater mineralisation with water residence times (modified after Bennett et al., 2022a). Note: The value after the well ID is the TDS value (in mg/L).

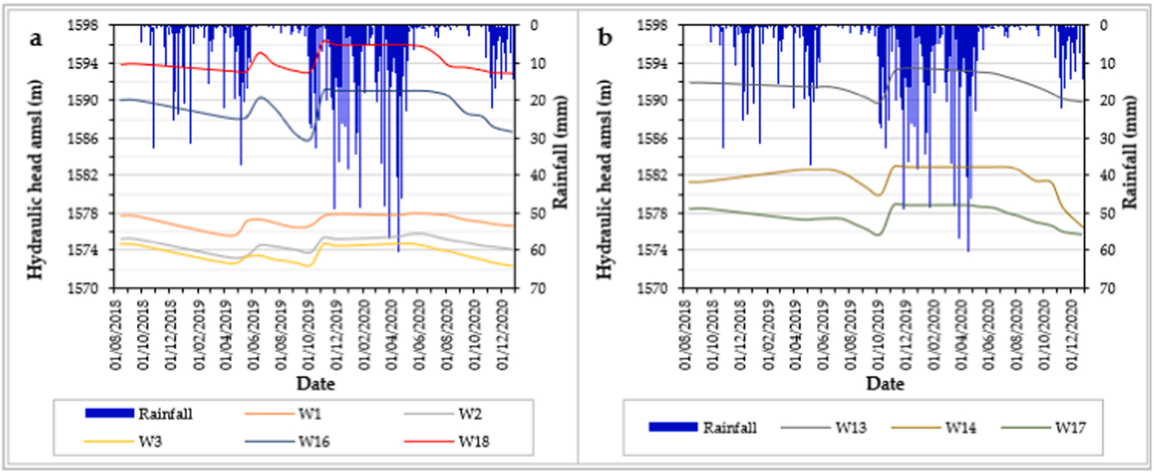

Fig. 8. Hydraulic head fluctuations at high elevations at Nkoasenga, and daily rainfall (Olmotonyi rainfall station) for the years 2018–2020.

followed by a recession in the dry period. This is comparable to W1, W2 and (to a lesser extent) W3, where the rise is delayed in W2. The rainy period in 2019–2020 was very wet. When the rains start in November 2019, there is an immediate rise of piezometric levels, which remain high and stable during this rainy season. The recession starts after a delay, in August 2020. Wells more to the north (W19 see Fig. 6b, W4 see Fig. 6c, and also W5 see Fig. 6d and W6′ see Fig. 6e) show an extra recharge wave after the end of the rains, in June 2020. The response of groundwater level to rainfall for Fig. 6e and f are low due to relatively large distances from the local recharge areas. The local flow system is controlling groundwater level in the area. At lower elevations, wells W6, W6' and W99 are in swampy areas, indicating groundwater discharge spots. Well W5 which is located at lower elevation and is much deeper (well depth = 26 m) compared to other wells (average well depth = 8 m) shows the rise of water level even during the dry season (Fig. 6d), this indicates a lag between rainfall and water level rise due to longer periods of travel time.

Table 1 summarises the basic descriptive statistics for the static water level measurements. At Nkoasenga, the wells at high elevations (from 1577 to 1598 m elevations) show high values of maximal fluctuation (average: 2.6 m) compared to wells at intermediate (average: 1.3 m) and lower elevations (average: 0.4 m), this indicates that the wells at high elevations are situated near the recharge area, hence they respond quickly to rainfall (Fig. 6a) and recharge to the maximum capacity during the rainy season but due to the sloping aquifer in the area, they lose a lot of water after the rainy season as the water is moving to the lower elevations. The high values of maximal fluctuation in the wells at high elevations compared to wells at intermediate and lower elevations could be also due to a possibility that the high elevation areas have a lower specific yield that causes a fast response compared to the middle and lower elevation areas.

Table 1
Basic descriptive statistics for static water level (SWL) measurements in the shallow aquifer on the northern flank of Ngurdoto crater for the years 2018–2020.

Region	Well ID	Elevation (m)	Well Depth (m)	Hydrological year 2018–2019						Hydrological year 2019–2020					
				Min. SWL (m)	Month	Max. SWL (m)	Month	Average SWL (m)	Maximal Fluctuation (m)	Min. SWL (m)	Month	Max. SWL (m)	Month	Average SWL (m)	Maximal Fluctuation (m)
Nkoasenga	W18	1598	5.0	2.92	June	4.89	May	4.3	2.0	1.72	Nov.	4.75	Oct.	3.0	3.0
	W13	1594	10.9	2.10	Oct.	3.70	Sept.	2.8	1.6	0.56	Dec.	4.12	Oct.	1.6	3.6
	W16	1591	10.0	0.77	June	4.73	Sept.	2.5	4.0	0.00	Nov.-June	5.06	Oct.	0.9	5.1
	W15	1587	8.4	1.23	Oct.	3.63	Sept.	1.9	2.4	0.53	Dec.	4.33	Oct.	1.7	3.8
	W14	1583	7.2	0.29	June	2.24	Sept.	1.0	2.0	0.00	Nov.-July	3.00	Oct.	0.5	3.0
	W17	1580	11.2	1.50	Oct.	3.68	Sept.	2.7	2.2	1.13	April	4.17	Oct.	1.9	3.0
	W1	1579	7.5	1.33	Oct.	3.34	April	2.1	2.0	1.07	June	2.30	Oct.	1.4	1.2
	W3	1578	7.8	3.35	Oct.	5.34	April	4.7	2.0	3.25	May	5.49	Oct.	3.9	2.2
	W2	1577	6.8	1.74	Oct.	3.74	April	2.8	2.0	1.20	June	3.17	Oct.	1.8	2.0
	W19	1560	7.2	1.56	June	1.95	Sept.	1.8	0.4	0.81	June	1.88	Oct.	1.2	1.1
	W99	1560	3.2	0.00	June	0.20	April	0.05	0.2	0.00	Oct.-Sept.	0.00	Oct.-Sept.	0.0	0.0
	W4	1479	4.3	1.12	Oct.	3.69	May	3.0	2.6	0.00	May-July	3.55	Oct.	1.1	3.6
	W5	1432	25.6	20.98	Sept.	21.44	Oct.	21.2	0.5	19.69	Sept.	21.04	April	20.4	1.4
	W6	1400	1.6	0.51	June	0.58	Oct.	0.5	0.07	0.22	July	0.37	Oct.	0.3	0.2
	W6’	1400	0.7	0.34	July-Aug.	0.37	June	0.3	0.03	0.00	May-July	0.36	Sept.	0.2	0.4
Leguruki	W10	1366	9.3	0.40	June	2.90	Sept.	1.3	2.5	0.00	April-Aug.	3.69	Oct.	0.5	3.7
	W7	1348	4.9	1.62	Oct.	4.38	April	2.8	2.8	0.00	May-June	2.40	Oct.	1.2	2.4
	W8	1348	5.4	1.25	Oct.	3.77	April	2.7	2.5	0.10	June	3.14	Oct.	1.3	3.0
	W9	1348	10.7	1.08	May	2.05	Oct.	1.3	1.0	0.30	June	4.46	Sept.	1.3	4.2

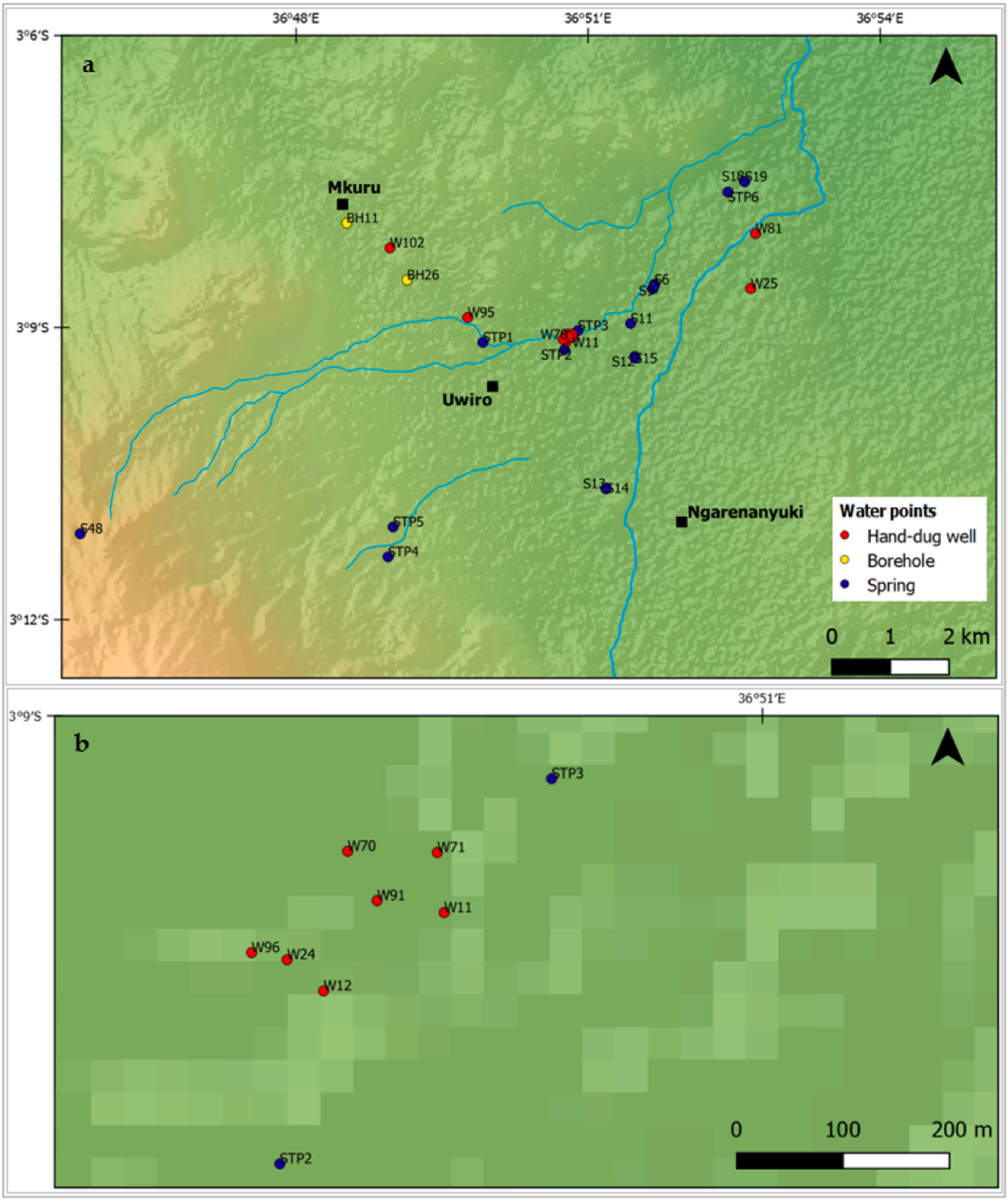

Fig. 9. (**a**) A zoomed-in part of Fig. 2 showing the spatial distribution of hand-dug wells, boreholes and springs on the north-eastern flank of Mount Meru used for investigating groundwater-level trends in the area, and (**b**) a zoomed-in part of figure (**a**) (i.e. Fig. 9a) showing the spatial distribution of hand-dug wells and springs at part of Uwiro.

3.2.2. North-eastern flank

Fig. 9 (which is a zoomed-in part of Fig. 2) shows the spatial distribution of hand-dug wells and springs on the north-eastern flank of Mount Meru used for investigating groundwater-level trends on this flank. At Uwiro, a perched aquifer has been identified at shallow depth (see Fig. 10). The perched aquifer at Uwiro is composed of debris avalanche deposits, whereas well W96, also, at Uwiro, is

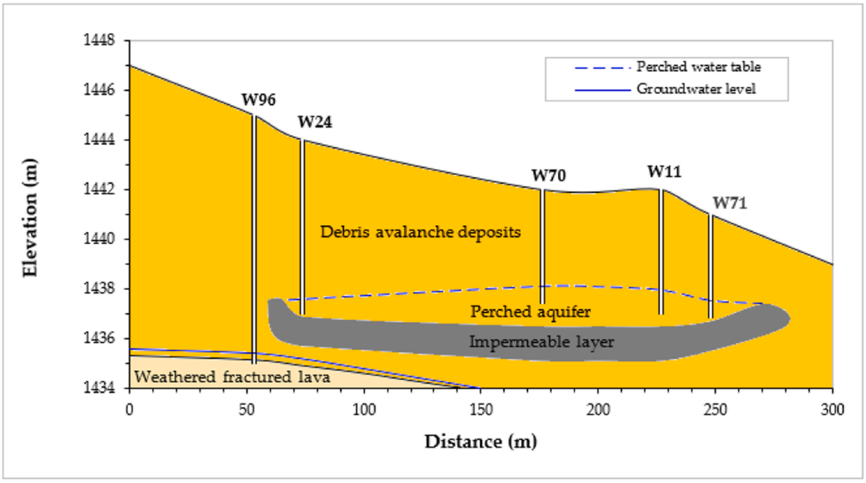

Fig. 10. Cross-section showing groundwater level at Uwiro, identifying a perched aquifer at shallow depth.

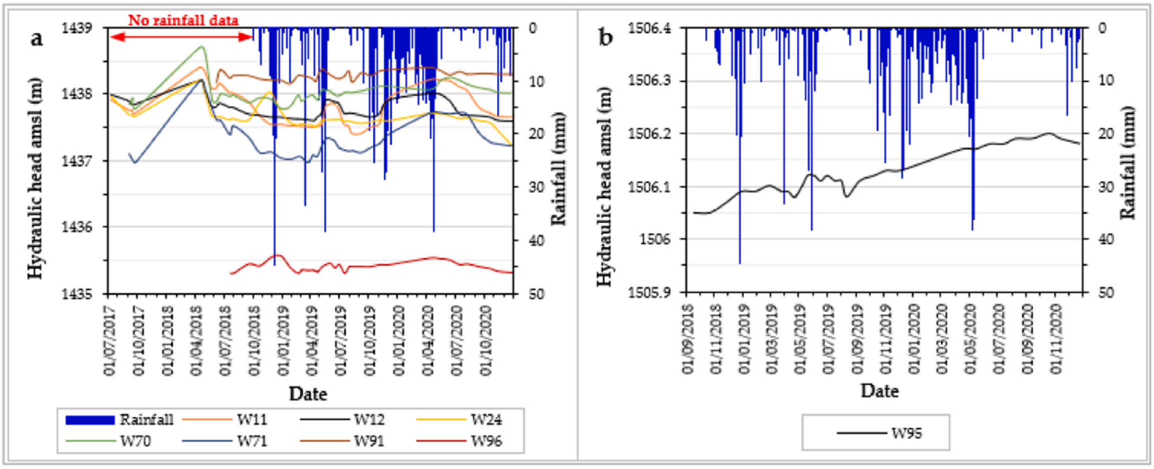

Fig. 11. Hydraulic head fluctuations at: (**a**) Uwiro and (**b**) W95 in Mkuru, and daily rainfall (Nariva school rainfall station) for the years 2017–2020.

withdrawing water from the semi-confined aquifer, composed of weathered fractured lava. The static water level in W24 is at shallow depth compared to W96, but groundwater cannot flow from W24 to W96 due to the elevation, this observation, together with the presence of an impermeable layer in W24 and W71 which prevented further digging of the wells make us to assume that there is a perched aquifer here. At Mkuru and Ngarenanyuki the aquifer is semi-confined, composed of weathered fractured lava (Bennett et al., 2022b).

Fig. 11 shows hydraulic head fluctuations on the north-eastern flank for the years 2017–2020. Also, the "dips" (dynamic water levels) in the time series data will not be considered in the analysis of fluctuations of static water level in the aquifer. Fig. 12 shows automatic groundwater level measurements using diver and barodiver recorded in W25. The diver measurements are clearly showing the evolution of static water level (the upper "curve"), and the pumping sessions (the "vertical" lines down). In the analysis of fluctuations of static water level in the aquifer, also, the downward peaks due to pumping sessions will not be considered. Fig. 13 shows the spring discharge fluctuation at Ngarenanyuki for two springs: S12 and S13 for the year 2019.

The perched aquifer at Uwiro which is at shallow depth (average water level = 4.5 m below the ground surface) responds quickly to rainfall; water level starts to rise soon after the start of the rains and decline shortly after the rains stop (see Fig. 11a), this indicates that the aquifer is locally recharged. However, the hydraulic head in this perched aquifer is very smooth compared to the rainfall in the area it receives (see Fig. 11a), this can be attributed to a small size of the perched aquifer which causes the amplitude of groundwater level fluctuation to settle at considerably low height, and stabilizes in a short time. The fluctuation amplitudes of static water level are more pronounced in year 2019–2020 than in 2018–2019 (see Fig. 11a), since the rainy season in 2019–2020 was wet while the rainy period in 2019–2020 was exceptionally dry. The fluctuation amplitudes of static water level in the semi-confined aquifer at Uwiro in W96 are lesser than the amplitudes of static water level in the perched aquifer (see Fig. 11a, and compare W96 with the other wells); this suggests that the amplitude of groundwater level fluctuation in W96 is affected by longer periods of travel time. Also, the semi-

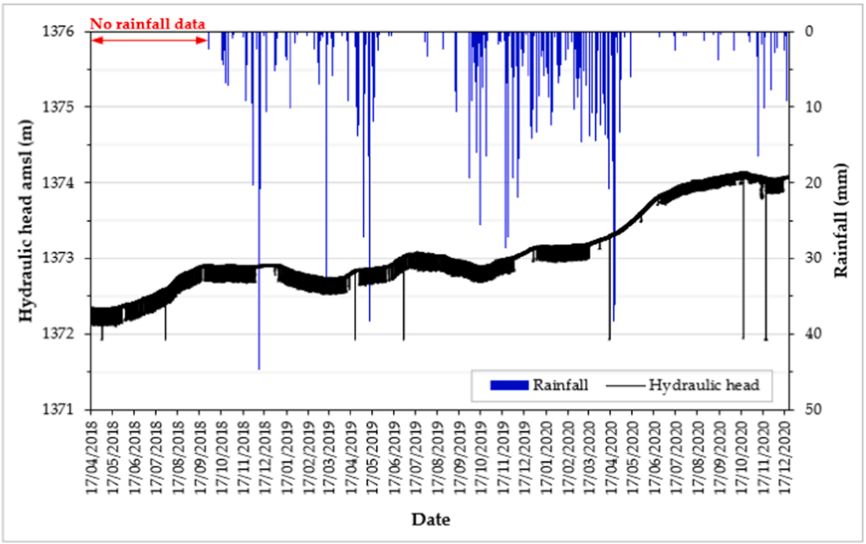

Fig. 12. Hydraulic head fluctuations (after barometric effect correction) at well W25 and daily rainfall (Nariva school rainfall station) for the years 2018–2020.

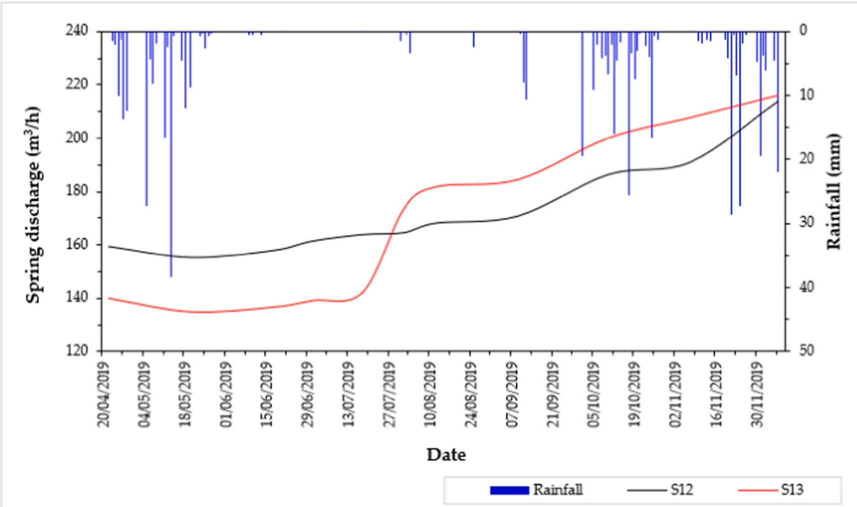

Fig. 13. Spring discharge fluctuation at Ngarenanyuki and rainfall (Nariva school rain station) for the year 2019.

confined condition of the aquifer in W96 can cause low response to rainfall due to limited water infiltration (low groundwater recharge) into the aquifer. The perched aquifer shows similar values for the average maximal fluctuations of static water level: 0.31 and 0.33 m for the two hydrological years: 2018–2019 and 2019–2020, respectively, whereas the semi-confined aquifer at W96 shows the values of 0.23 and 0.13 m for the maximal fluctuations of static water level in the two hydrological years, respectively; the values are slightly lower than those of the perched aquifer. The semi-confined aquifer at Mkuru which is slightly deeper (located 19 m below the ground surface (Bennett et al., 2022b)) than the perched aquifer at Uwiro shows very small values of maximal fluctuations of static water level (average: 0.07 m (7 cm)), and the water level continues to rise even during the dry season (see Fig. 11b), this indicates a lag between rainfall and water level rise. For the two hydrological years: 2018–2019 and 2019–2020, the semi-confined aquifer at Mkuru in well W95 shows similar values for the maximal fluctuations of static water level: 0.07 and 0.08 m, respectively. There is a rise of about 0.15 m (15 cm) between the static water level in September 2018 and October 2020 (see Fig. 11b). Moreover, the low response to rainfall in W95 is attributed to the semi-confined condition in the area which cause limited water infiltration (low groundwater recharge) into the aquifer. Also, the low hydraulic conductivity (K) of this semi-confined aquifer (K= 0.41 m/d) (Bennett et al., 2022b) causes low response to rainfall due to low recharge. For the well W25 at Ngarenanyuki, which is located at lower elevation (see Fig. 14) and slightly deeper (well depth: 27 m, with average water level at 26 m below the ground surface), also, here the lag between rainfall and water level rise is observed as the groundwater level continues to rise even during the dry season (see Fig. 12). In well W25, the

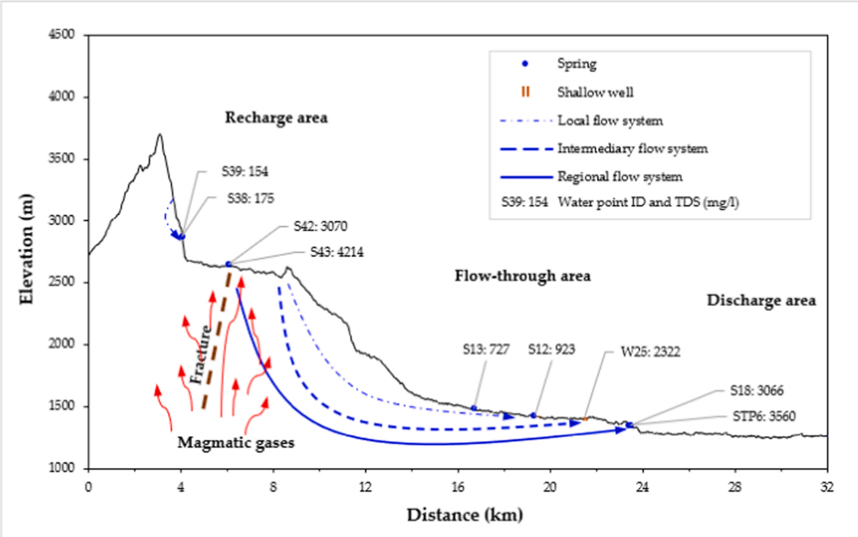

Fig. 14. Cross-section showing the simplified groundwater flow conceptual model for the north-eastern flank of Mount Meru (modified after Bennett et al., 2022a).

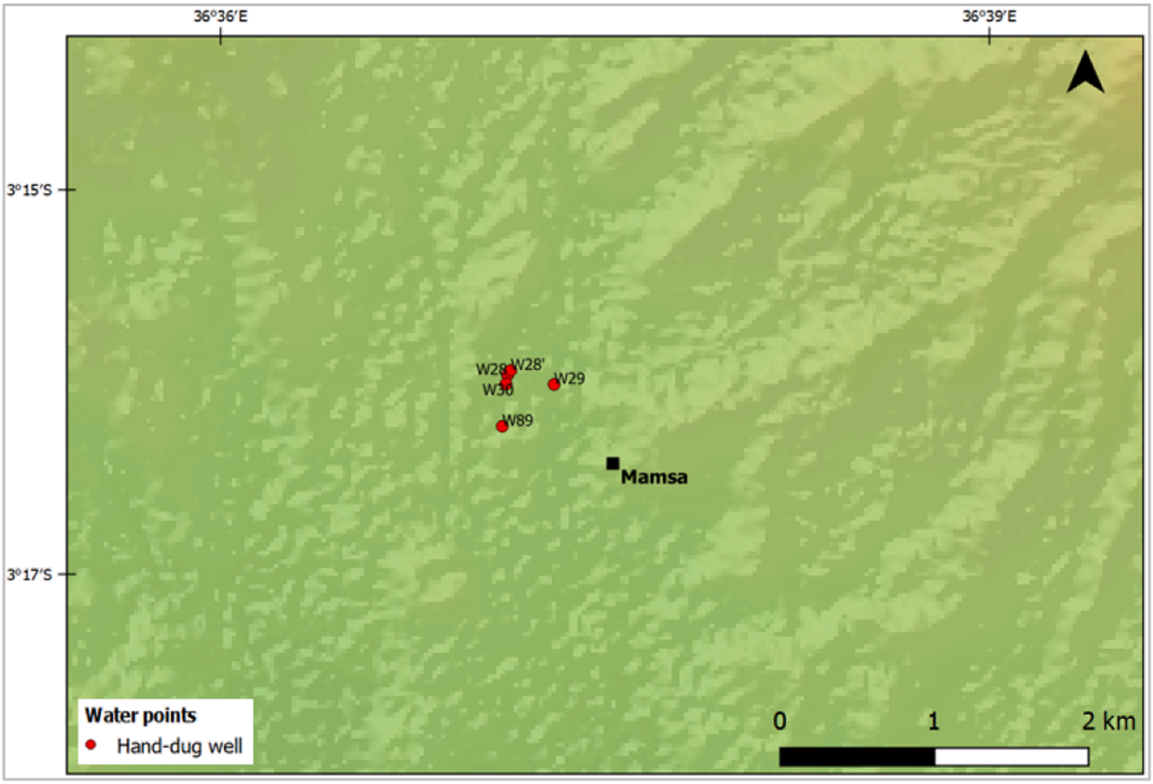

Fig. 15. A zoomed-in part of Fig. 2 showing the spatial distribution of hand-dug wells on the western flank of Mount Meru used for investigating groundwater-level trends in the area.

maximal fluctuations of static water level for the two hydrological years: 2018–2019 and 2019–2020 are 0.30 and 1.20 m, respectively. There is a rise of about 1.80 m between the static water levels in April 2018 and December 2020; with an increase of 1.20 m occurring during the hydrological year 2019–2020 (see Fig. 12). The lag between rainfall and water level rise is also observed at lower elevations on the two springs: S12 and S13, the discharges start to rise after approximately two months' time lag (mid-June) after the start of heavy rains at mid-April and continue to rise through the dry season until the next rainy season (see Fig. 13). It is quite

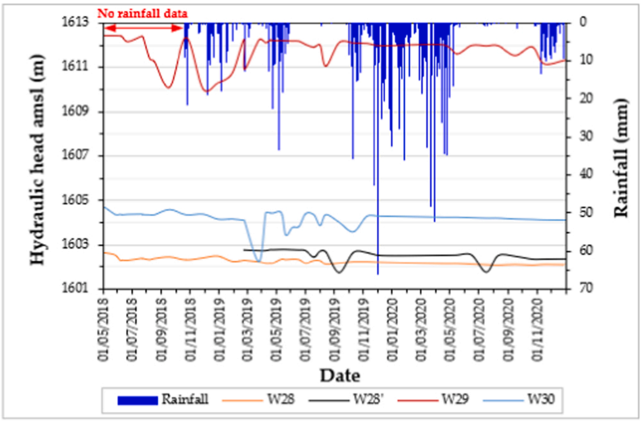

Fig. 16. Hydraulic head fluctuations at Mamsa and daily rainfall (Mamsa rainfall station) for the years 2017–2020.

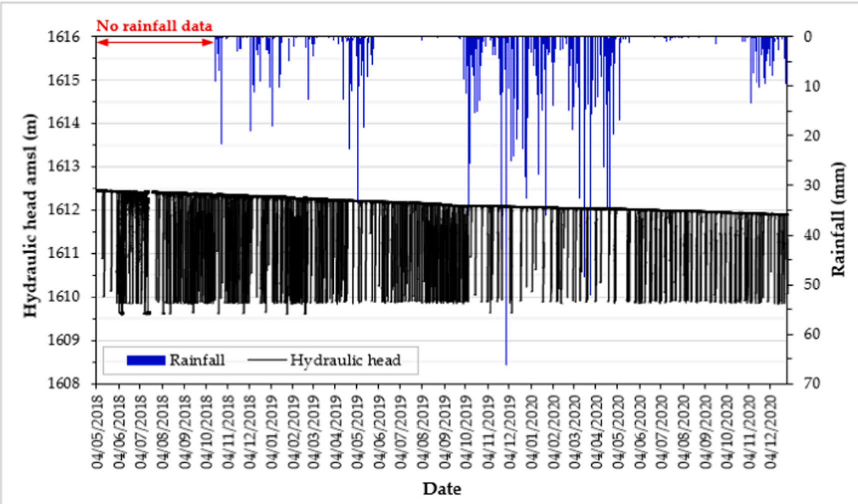

Fig. 17. Hydraulic head fluctuations (after barometric effect correction) at well W29 and daily rainfall (Mamsa rainfall station) for the years 2018 – 2020.

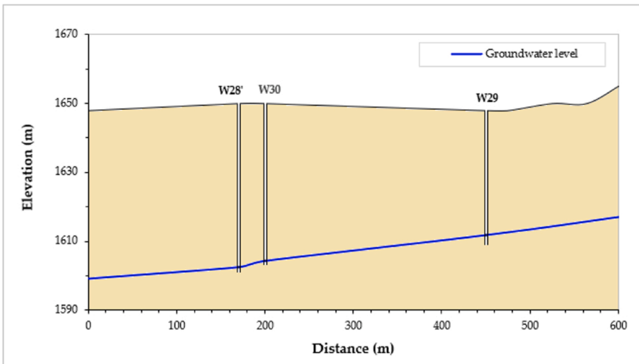

Fig. 18. Cross-section showing groundwater level at Mamsa.

interesting to see how S12 shows a gradual increase of discharge, while S13 shows a sudden large increase in July (corresponding to rainfall in April-May). It would require a longer time series data to make a conclusion on this, but for now, this can be attributed to a preferential water flow path along S13, which receives slightly more local recharge than the flow path along S12.

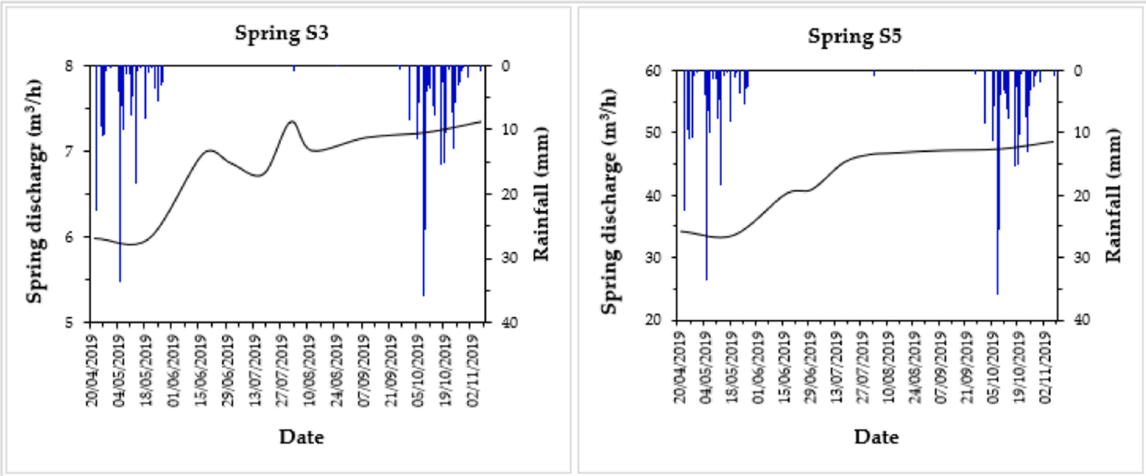

Fig. 19. Spring discharge fluctuation at Oldonyo Sambu (north-western flank) and rainfall (Mamsa rain station) for the year 2019 (Bennett et al., 2021).

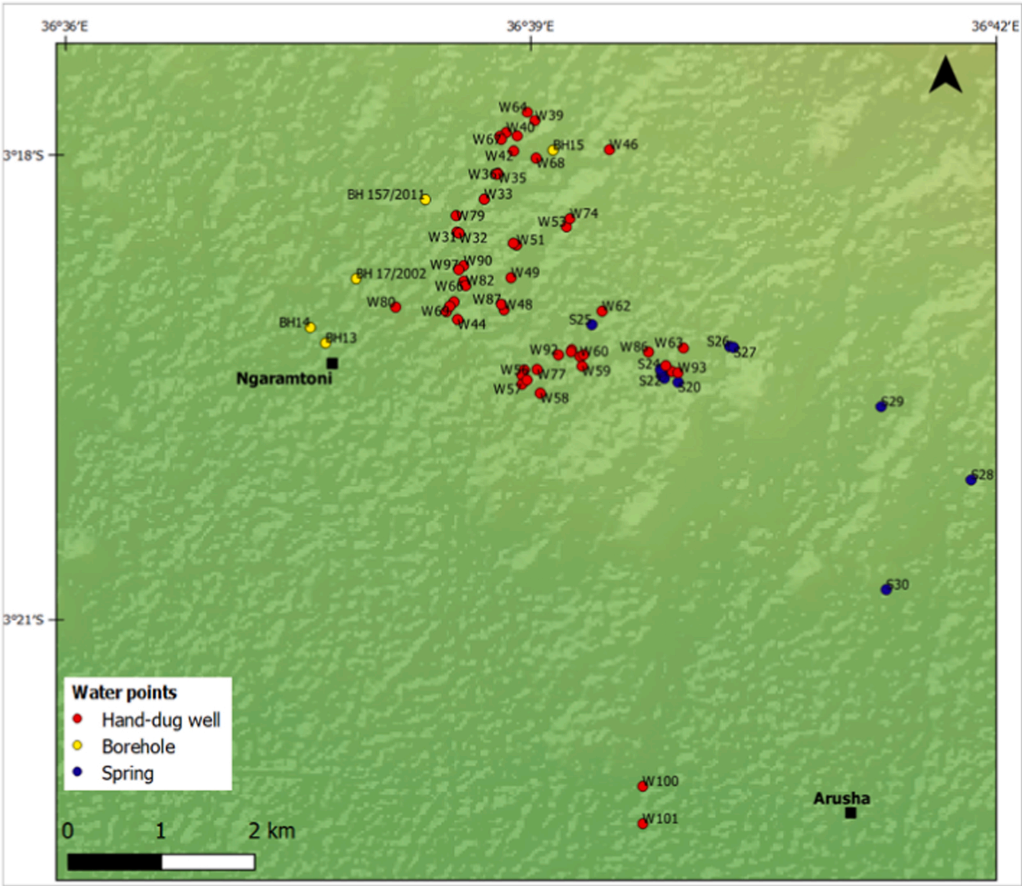

Fig. 20. A zoomed-in part of Fig. 2 showing the spatial distribution of hand-dug wells, boreholes and springs on the south-western flank of Mount Meru used for investigating groundwater-level trends in the area.

3.2.3. Western flank

Fig. 15 (which is a zoomed-in part of Fig. 2) shows the spatial distribution of hand-dug wells on the western flank of Mount Meru used for investigating groundwater-level trends on this flank. The annual rainfalls (in mm/year) on this flank for the years 2019 and

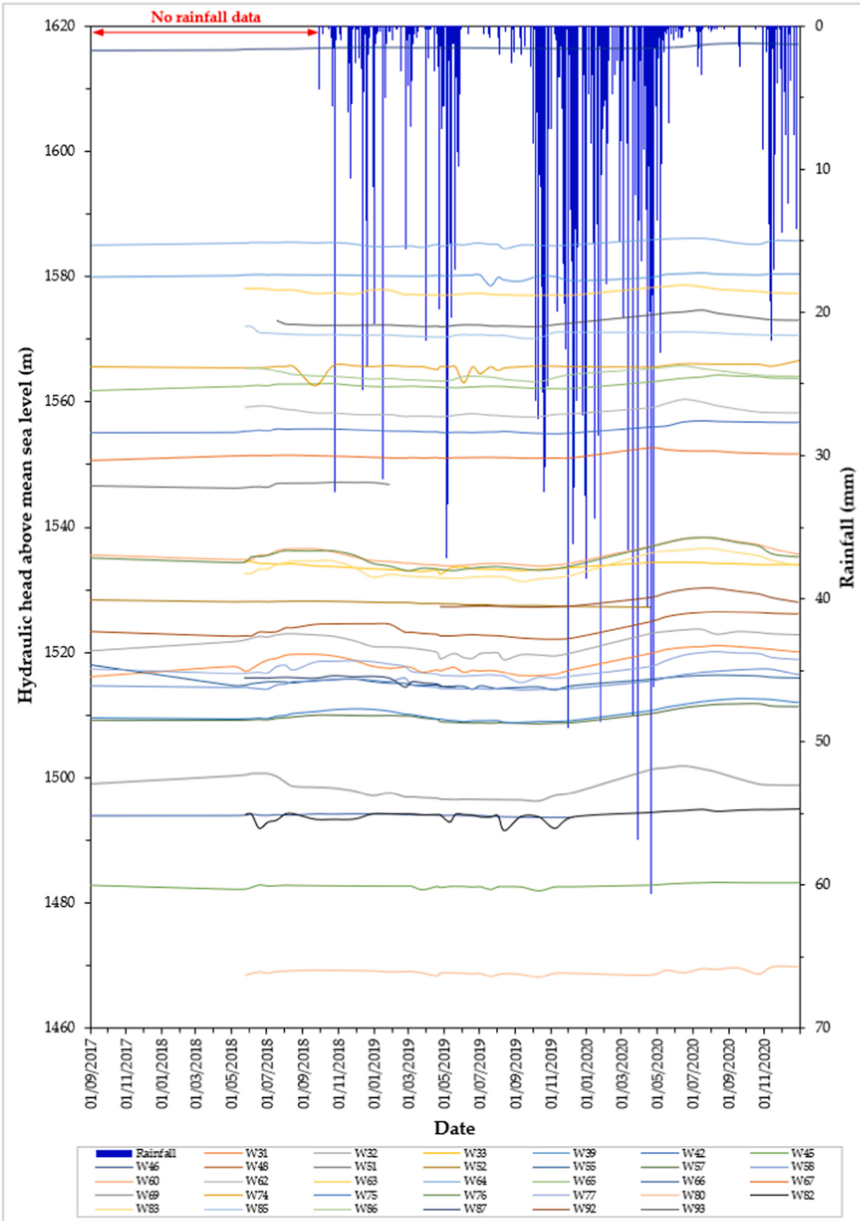

Fig. 21. Hydraulic head fluctuations at Ngaramtoni and daily rainfall (Olmotonyi rainfall station) for the years 2017–2020.

2020 are 896 and 914 respectively. Fig. 16 shows hydraulic head fluctuations in the four hand-dug wells at Mamsa on the western flank for the years 2017–2020, and Fig. 17 shows automatic groundwater level measurements recorded in W29, one of the four wells. The four wells are regularly pumped. The manual measurements (Fig. 16) are sometimes affected by pumping: this is clear from the diver measurements (Fig. 17). The "dips" are just influenced by pumping. This shows how extremely useful and important the diver measurements are here: they have allowed to distinguish this. The diver measurements show very clearly that the static water levels (that is the top line that can be drawn on the diver measurements: in this case a linear, almost constant line, with a slight dip), and in the other three wells, static level is almost constant, linearly decreasing a bit with time. During pumping session in W29 (Fig. 17), water level is reduced by 2.5–3 m, gradually decreasing to 2 m. This is simply controlled by the pump position in the well: as we can see, it is a constant level to which the water level is lowered (with just a few disturbances – stirring or moving of pump). Also, the "dips" in the time series of manual measurements, and pumping sessions (the "vertical" lines down) in the time series of automatic measurements, will not be considered in the analysis of fluctuations of static water level in the aquifer. By considering the diver measurements (Fig. 17), the static water levels for the two hydrological years: 2018–2019 and 2019–2020 decrease by 0.25 and 0.15 m, respectively. There is a decrease of about 0.50 m between the static water levels in May 2018 and December 2020, this can be attributed to low/

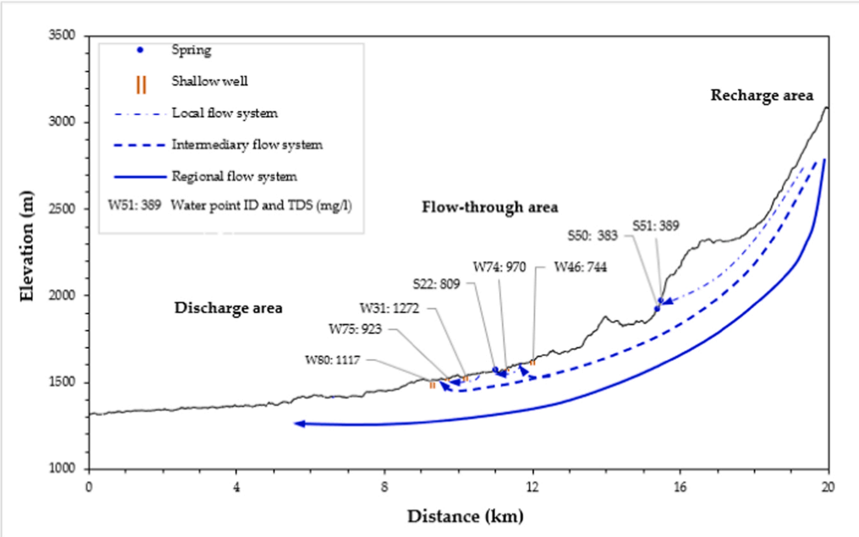

Fig. 22. Cross-section showing the locations of the five automatically monitored wells, and a simplified groundwater flow conceptual model for the south-western flank of Mount Meru showing the increase of groundwater mineralisation with water residence times (modified after Bennett et al., 2022a).

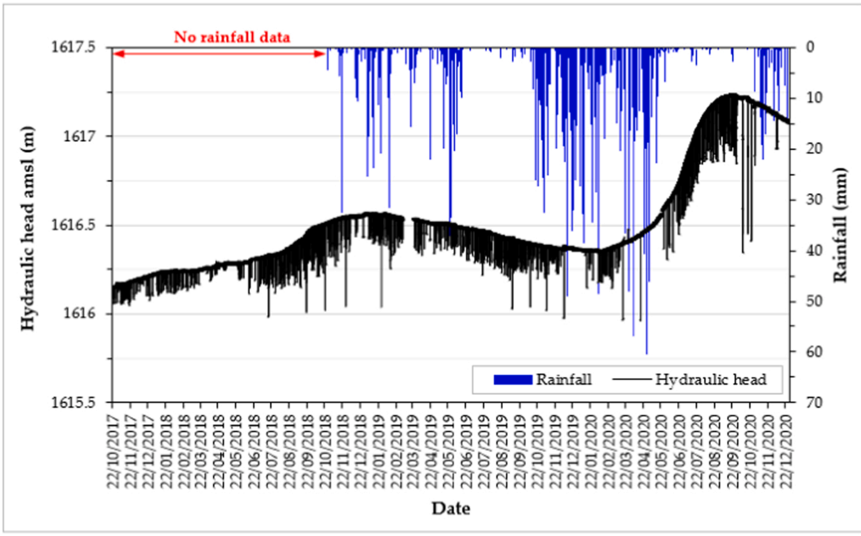

Fig. 23. Hydraulic head fluctuations (after barometric effect correction) at well W46 and daily rainfall (Olmotonyi rainfall station) for the years 2017 – 2020.

reduced recharge, or exploitation. The low recharge in this aquifer can be attributed to its very low hydraulic conductivity (K= 0.15 m/d) (Bennett et al., 2022b). Therefore, the current pumping practices in the aquifer on the western flank should be restrained for sustainable groundwater management.

Fig. 18 shows a cross-section showing groundwater level in the area. The aquifer in this area is semi-confined, composed of weathered fractured lava (Bennett et al., 2022b). The wells are in lower elevation far away from the recharge area (Bennett et al., 2022a), and the water table is deeper (average static water level: 44 m below the surface) compared to the other flanks. The wells did not show any response to rainfalls (Fig. 16), this is attributed to a semi-confined condition of the aquifer in the area. This clearly shows that recharge is remote, and with long travel times together with low hydraulic conductivity of the aquifer, homogenising seasonal variations. The lag between rainfall and water level rise is observed on the two springs: S3 and S5 at Oldonyo Sambu (north-western flank, > 10 km far from Mamsa) (see Fig. 19), their discharges which are controlled by a relatively shallow flow system (local flow system) compared to that controlling groundwater level in wells at Mamsa (intermediary flow system) start to rise after approximately a month time lag (mid-May) after the start of heavy rains at mid-April, and continue to rise through the dry season until the next rainy season. The springs are relative closer to the recharge area compared to the wells at Mamsa (Bennett et al., 2022a).

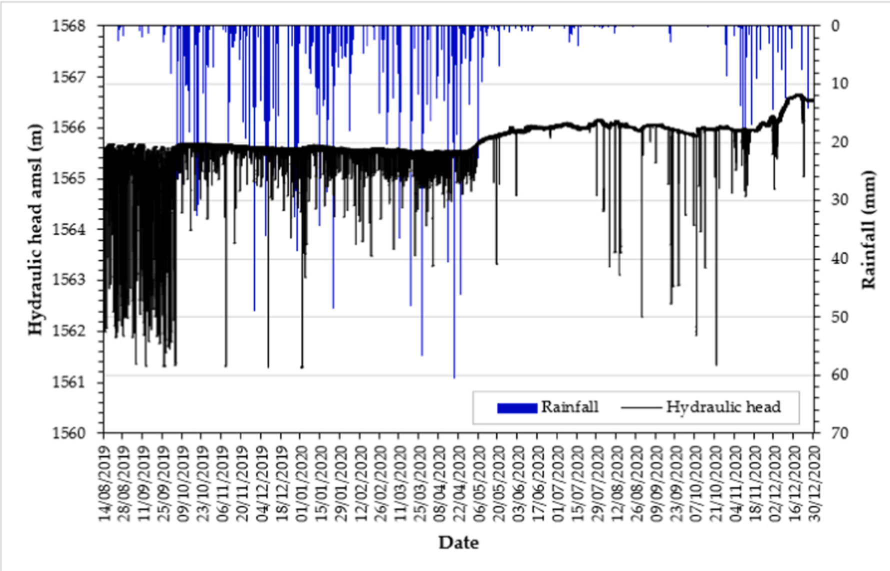

Fig. 24. Hydraulic head fluctuations (after barometric effect correction) at well W74 and daily rainfall (Olmotonyi rainfall station) for the years 2019 – 2020.

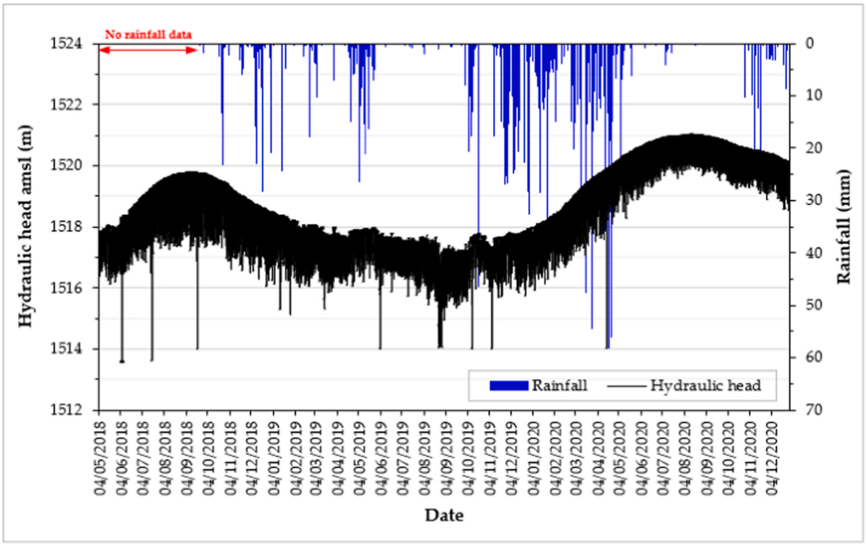

Fig. 25. Hydraulic head fluctuations (after barometric effect correction) at well W31 and daily rainfall (ASA Farm rainfall station) for the years 2018 – 2020.

3.2.4. South-western flank

Fig. 20 (which is a zoomed-in part of Fig. 2) shows the spatial distribution of hand-dug wells, boreholes, and springs on the south-western flank of Mount Meru used for investigating groundwater-level trends on this flank. The topmost part of the aquifer, exploited by hand-dug wells, is composed of pyroclastics, whereas the deeper part of the aquifer, captured by boreholes, is composed of weathered fractured lava and weathered pyroclastics (Bennett et al., 2022b).

Fig. 21 shows hydraulic head fluctuations on the south-western flank for the years 2017–2020, while Fig. 22 shows the locations of the five automatically monitored wells, and a simplified groundwater flow conceptual model for the south-western flank modified after Bennett et al. (2022a).

Fig. 21 represents all the wells monitored on the south-western flank to compare fluctuation amplitudes between different wells (just to have a general overview of the fluctuation amplitudes between different wells). The general overview in Fig. 21 is that the wells at high and lower elevations show small values of maximal fluctuations of static water level compared to the wells at intermediate elevations. The wells are located far away from the recharge area and the intermediary flow system is mainly controlling groundwater

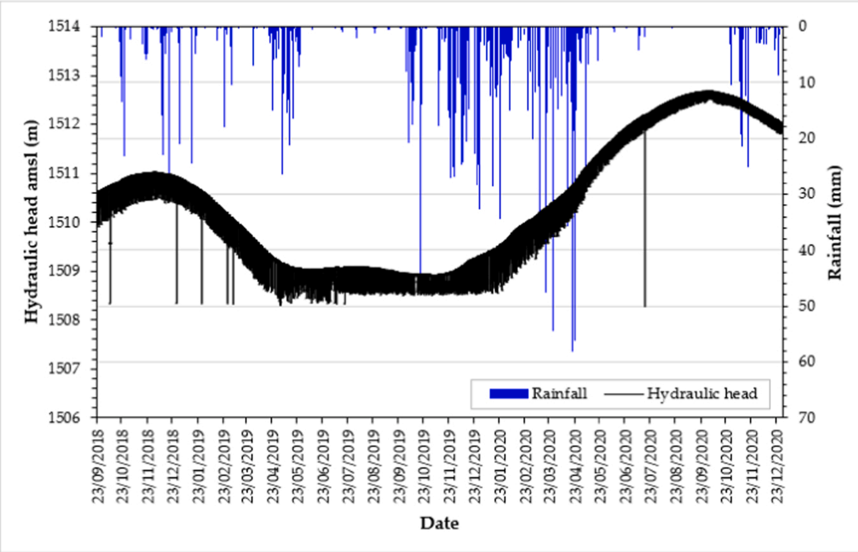

Fig. 26. Hydraulic head fluctuations (after barometric effect correction) at well W75 and daily rainfall (ASA Farm rainfall station) for the years 2018 – 2020.

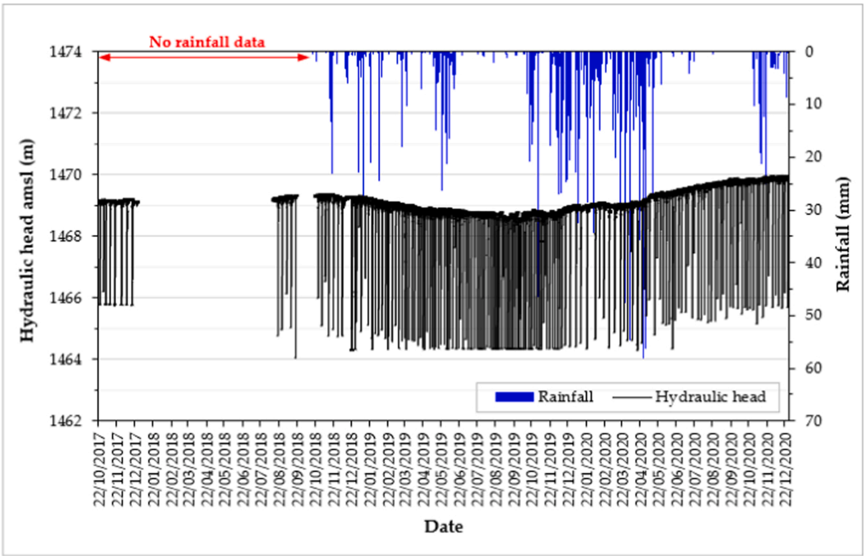

Fig. 27. Hydraulic head fluctuations (after barometric effect correction) at well W80 and daily rainfall (ASA Farm rainfall station) for the years 2017 – 2020.

flow in the area, but local flow systems playing role in some parts.

The automatic groundwater level measurements recorded in the five wells, in the descending order of their elevation, are shown in Fig. 23 (for W46 at 1631 m elevation), Fig. 24 (for W74 at 1575 m elevation), Fig. 25 (for W31 at 1534 m elevation), Fig. 26 (for W75 at 1524 m elevation) and Fig. 27 (for W80 at 1502 m elevation). In Figs. 23–27, the spikes of hydraulic head fluctuation with an interval of the small-time step can be observed, this can be clearly seen in Fig. 28b (part of diver measurements in W29), this is because the barometric pressure in the study area shows two maxima and two minima daily fluctuations (see Fig. 28a) due to warming/cooling of atmosphere, this is common in the tropics. The small daily fluctuations that still see on compensated series (see Fig. 28c) are "remainders" of these barometric fluctuations.

The year 2018 was a driest year (annual rainfall: 680 mm/year) compared to years 2019 (annual rainfall: 1105 mm/year) and 2020 (annual rainfall: 1104 mm/year), hence most of the wells did not show significant water level response to rains in the year 2018. For the years 2019–2020, one of the five automatic monitored wells, W46, which is slightly at higher elevation than the rest, shows that the groundwater level start to rise after approximately five months' time lag (late February 2020) after the start of heavy rains (early

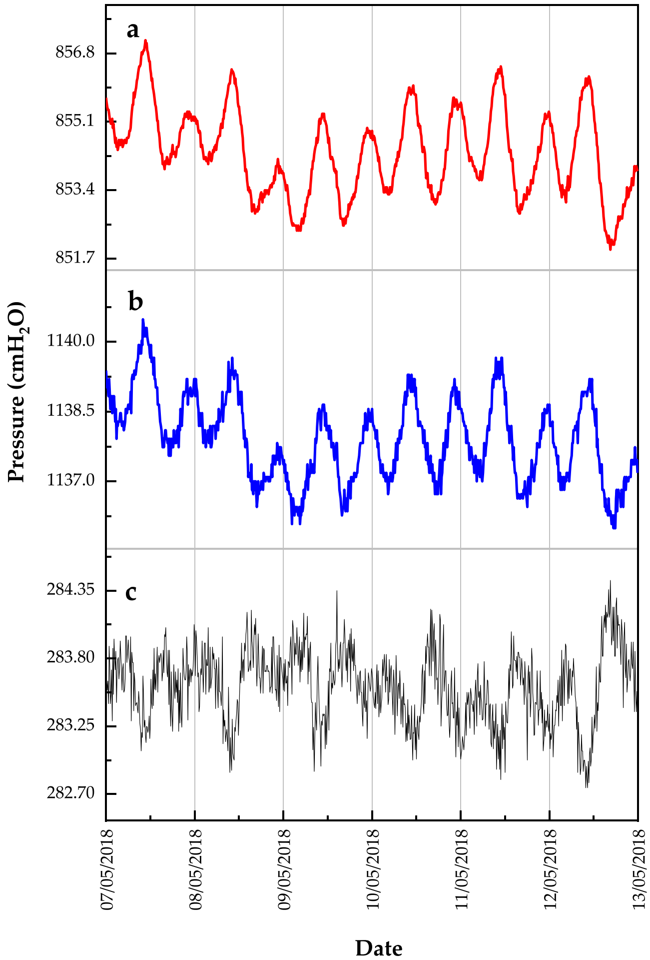

Fig. 28. (a) Barometric pressure (b) Pressure in well, and (c) Compensated series for diver/barodiver measurements recorded in well W29.

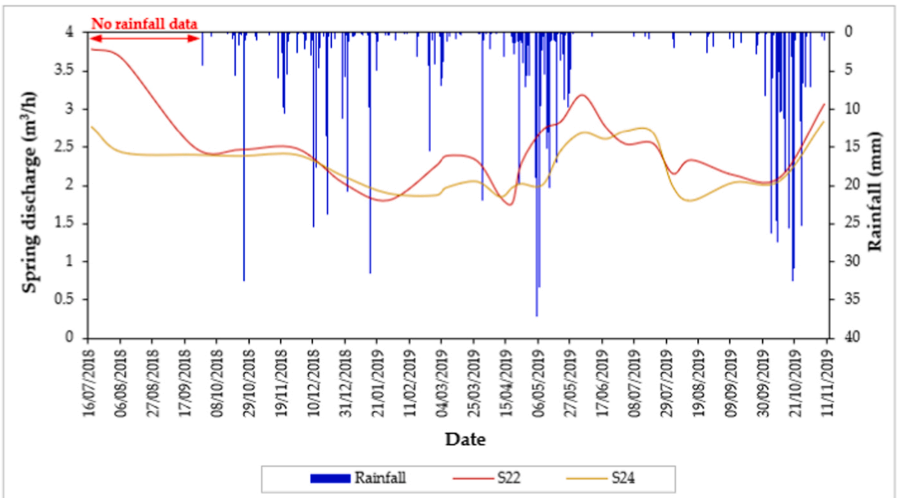

Fig. 29. Spring discharge fluctuation at Ngaramtoni and rainfall (Olmotonyi rain station) for the years 2018 – 2019.

Table 2
Basic descriptive statistics for static water level (SWL) measurements in the automatically monitored wells on the south-western flank of Mount Meru for the years 2018–2020.

Well ID	Elevation (m)	Well Depth (m)	Hydrological year 2018–2019						Hydrological year 2019–2020					
			Min. SWL (m)	Month	Max. SWL (m)	Month	Average SWL (m)	Maximal Fluctuation (m)	Min. SWL (m)	Month	Max. SWL (m)	Month	Average SWL (m)	Maximal Fluctuation (m)
W46	1631	15.7	14.5	Jan.	14.6	Sept.	14.5	0.1	13.8	Sept.	14.7	Jan.-Feb.	14.4	0.9
W74	1575	14.4							8.9	Aug.	9.5	April	9.2	0.6
W31	1534	22.8	14.3	Oct.	16.7	Sept.	15.9	2.4	13.0	Aug.	16.5	Nov.	14.6	3.5
W75	1524	16.1	13.0	Nov.-Dec.	15.0	June	14.1	2.0	11.3	Sept.	15.1	Nov.	13.4	3.8
W80	1502	38.8	32.6	Oct.-Nov.	33.4	Aug.	33.0	0.8	32.2	Sept.	33.3	Oct.	32.8	1.1

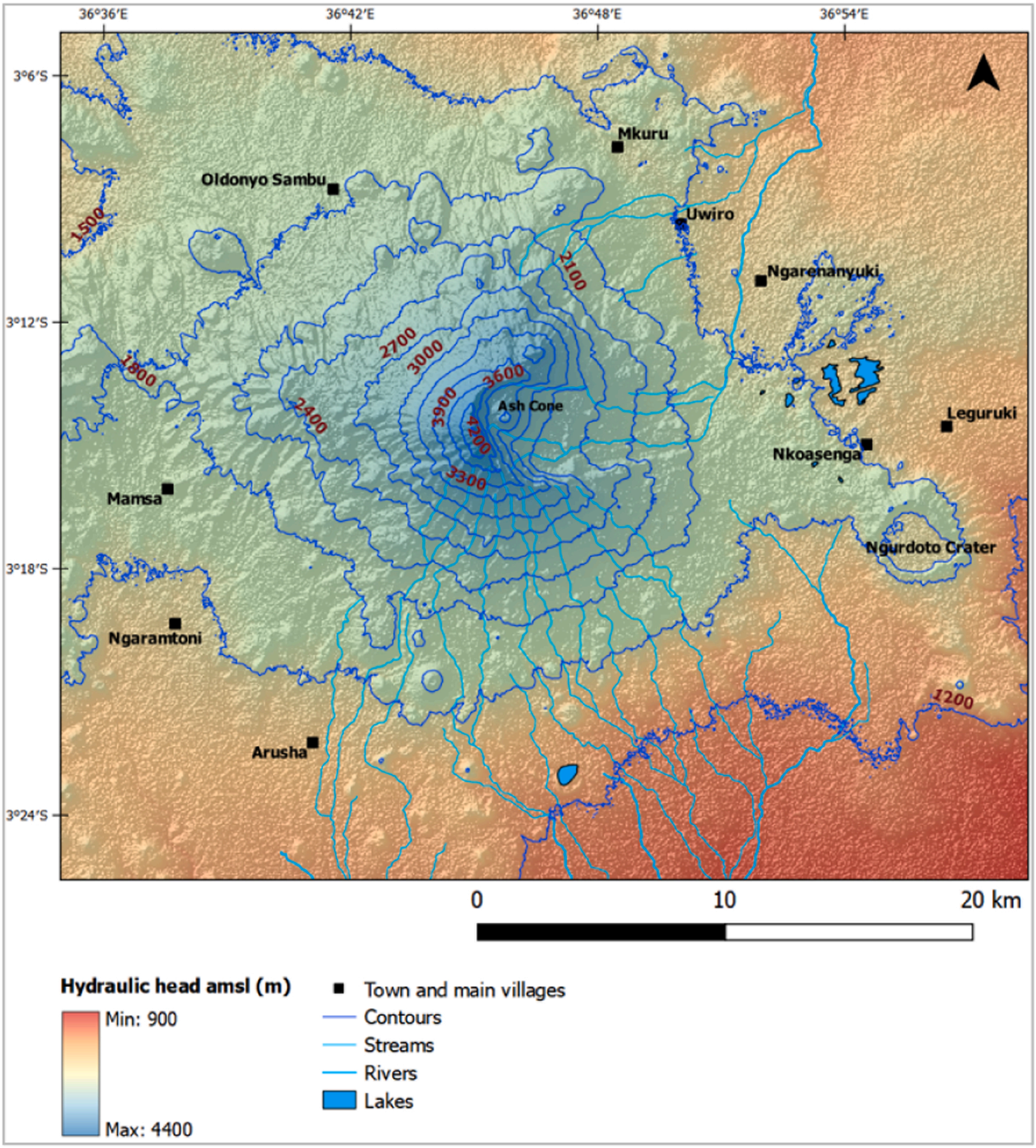

Fig. 30. A large (regional) scale piezometric map for the shallow aquifer in the study area.

October 2019), and continue to rise for approximately four months (up to late September 2020) after the end of heavy rains (late May 2020) (see Fig. 23), this indicates lag between rainfall and water level rise as the well is distant from the upstream localised recharge area, since the intermediary flow system is controlling the groundwater flow at this point. For the other four automatic monitored wells: W74 (see Fig. 24), W31 (see Fig. 25), W75 (see Fig. 26) and W80 (see Fig. 27), the local flow systems cause groundwater level to rise immediately after the start of heavy rains due to the localised recharge, whereas the intermediary flow system is controlling the continuation of the water level rise during the dry season because of the time lag. The smooth rise/decline of groundwater levels shown in the automatic measurements are caused by a high hydraulic diffusivity.

The influence of local flow systems in the lower elevations is also observed on the two springs: S22 and S24 (see Fig. 29), their discharges start to rise immediately after the start of rainfall and decline immediately after the end of the rainy season, indicating that

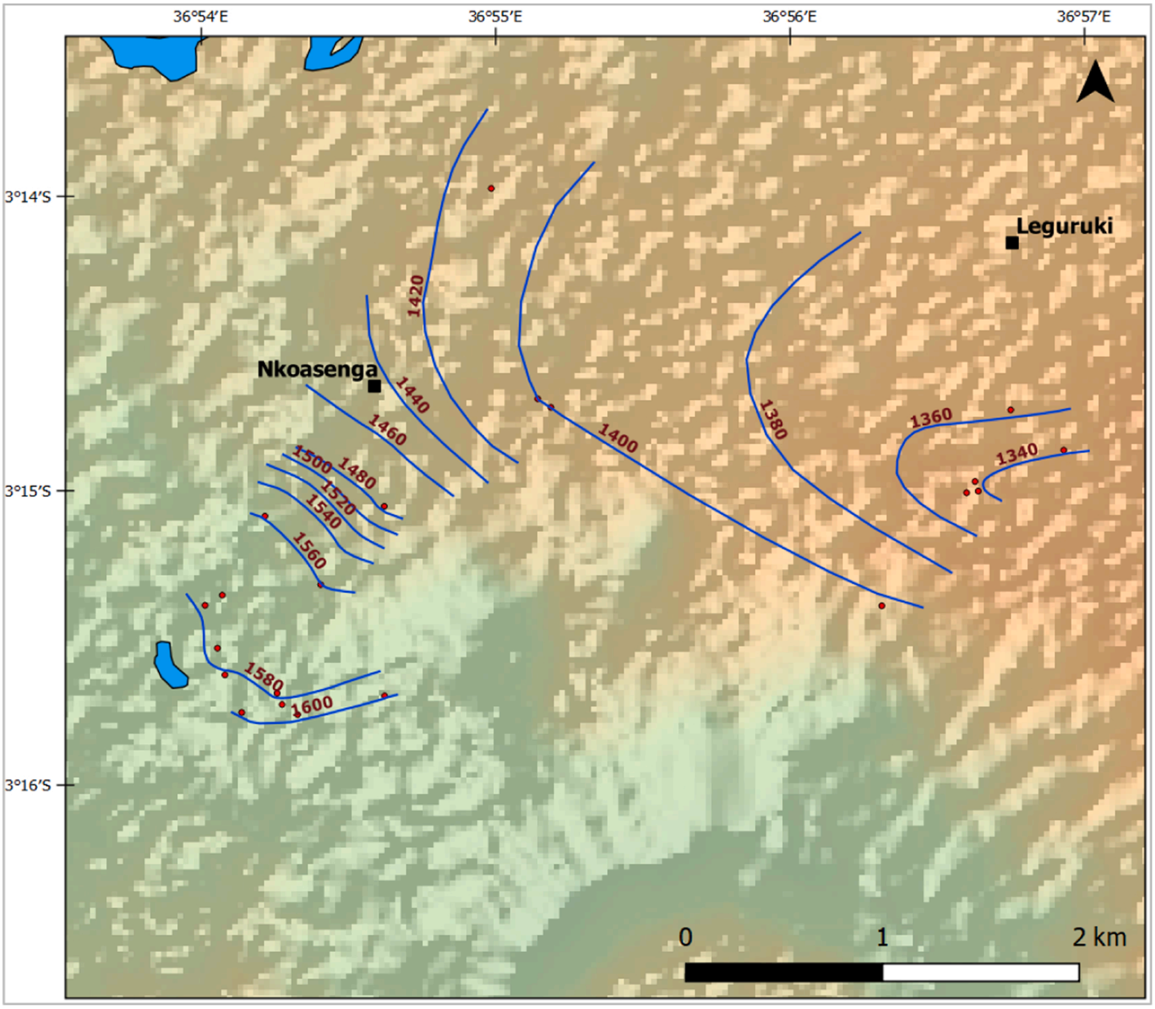

Fig. 31. Hydraulic head map showing contour lines of static water level in the shallow aquifer on the northern flank of Ngurdoto crater (Red small circles indicate the location of the wells).

the springs receive local recharge (Bennett et al., 2021), but the cycles of increase and decrease of the discharges during the dry season suggest different lags from the upstream localised recharge areas.

Table 2 summaries basic descriptive statistics for static water level measurements in the automatically monitored wells on the south-western flank of Mount Meru. The wells at high elevations (W46 and W74) show small values of maximal fluctuations of static water level (range: 0.1–0.9 m) compared to the wells at intermediate elevations (W31 and W75) (range: 2.0–3.8 m) (see Table 2); this is due to the fact that the wells at high elevations are located at relatively large distances from the upstream localised recharge areas (Bennett et al., 2022a), here the intermediary flow system is controlling groundwater flow (with less or no influence from nearby secondary localised recharges). Also, the high values of maximal fluctuation in wells at intermediate elevations compared to the wells at high elevations could be also due to high hydraulic conductivities at intermediate elevations (K: average = 3.6 m/d) compared to the hydraulic conductivity at high elevations (K = 1.9 m/d) (Bennett et al., 2022b), and due to the influence of the secondary localised recharges in these areas (local flow systems) (Bennett et al., 2022a). At lower elevation, W80 shows small values of maximal fluctuations of static water level (range: 0.8–1.1 m) compared to the wells at intermediate elevations (W31 and W75) despite the influence of the local flow systems in the lower elevations (Bennett et al., 2022a); this can be attribute to a very low hydraulic conductivity at W80 (K = 0.06 m/d) compared to hydraulic conductivities at W31 (K = 0.2 m/d) and W75 (K = 3.3 m/d).

Groundwater flow on and around Mount Meru is occurring in shallow water table aquifers with a varied volcanic lithology on the slopes of the mountain. In the study area, the semi-confined aquifers composed of weathered fractured lava on the north-eastern and western flanks show low or no response to rainfall, this is due to their semi-confined conditions which cause limited water infiltration hence low groundwater recharge. Also their low or no response to rainfall is attributed to their low hydraulic conductivities. The unconfined aquifer on the south-western flank shows variable responses to rainfall; the wells at intermediate elevations show high response to rainfall compared to the wells at high and lower elevations due to high hydraulic conductivities this zone.

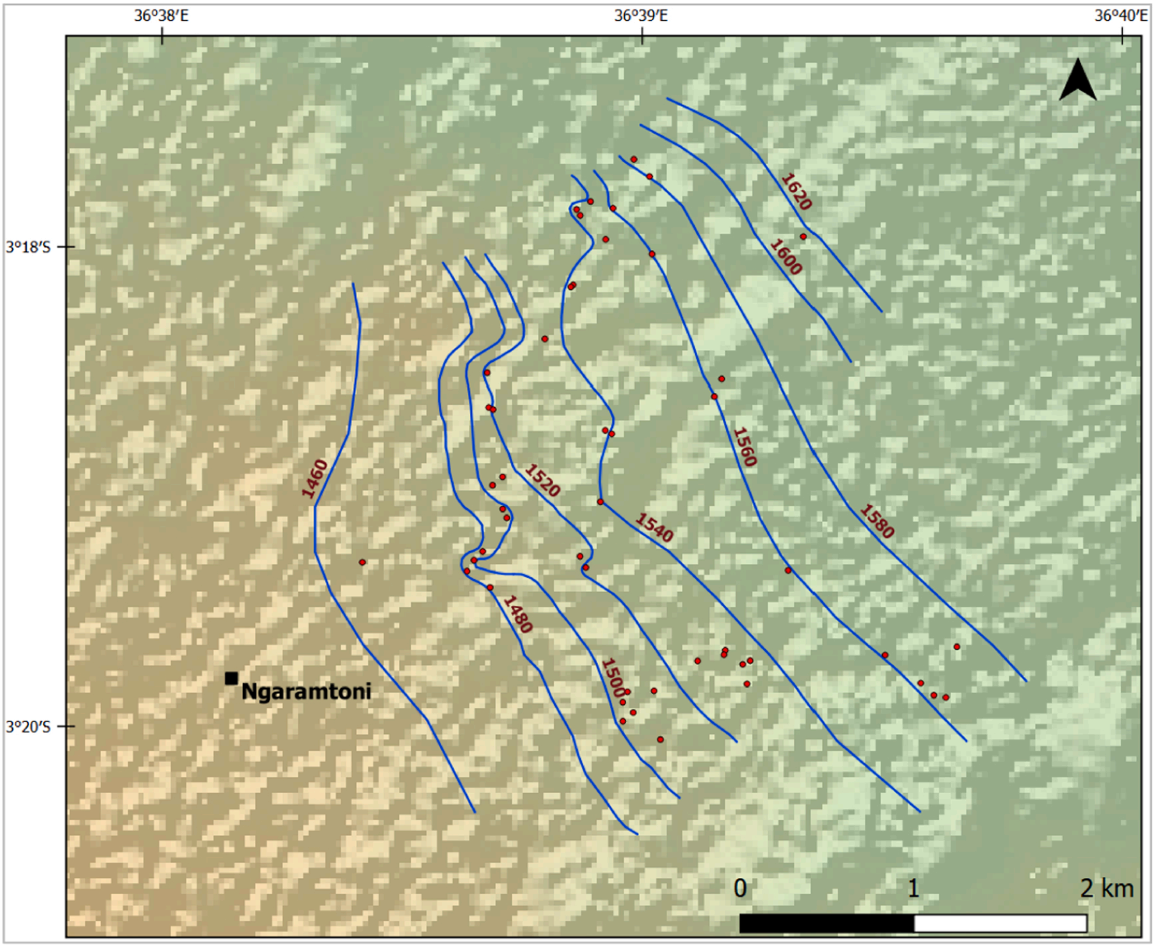

Fig. 32. Hydraulic head map showing contour lines of static water level in the shallow aquifer on the south-western flank of Mount Meru (Red small circles indicate the location of the wells).

3.3. Contour map of piezometric surface

Fig. 30 shows a large (regional) scale piezometric map for the shallow aquifer in the study area. The map was constructed by subtracting the average water depths in the study area from the Digital Elevation Model (DEM) of the area. The DEM provides the ground elevations, whereas the average water depths in the study area were obtained by interpolation of average water depths (under static water condition) at inventoried, and control points by using the inverse distance weighting (IDW) method. The geomorphology of the landscape in the area plays a great role in controlling the groundwater flow paths. The general groundwater flow system is involving a multidirectional flow from the highlands towards the lowlands.

Fig. 31 shows the hydraulic head map showing contour lines of static water level in the shallow aquifer on the northern flank of Ngurdoto crater. The map was constructed based on average static water level measurements in 21 shallow wells. Fig. 32 shows the hydraulic head map showing contour lines of static water level in the shallow aquifer on the south-western flank of Mount Meru. The map was constructed based on average static water level measurements in 49 shallow wells. The small (local) scale groundwater flow systems in the area are also involving multidirectional flows from the highlands towards the lowlands.

4. Conclusions and recommendations

Groundwater flow on and around Mount Meru is occurring in shallow water table aquifers with a varied volcanic lithology on the slopes of the mountain. The semi-confined aquifers composed of weathered fractured lava on the north-eastern and western flanks of the mountain show low or no response to rainfall due to their semi-confined conditions (which limit water infiltration) as well as due to their low hydraulic conductivities. The unconfined aquifer on the south-western flank shows variable responses to rainfall with wells at intermediate elevations showing high response to rainfall compared to the wells at high and lower elevations due to their high hydraulic conductivities. On the north-eastern flank, at Ngarenanyuki, there is a rise of about 1.80 m between the static water levels in April 2018 and December 2020 in the shallow aquifer, whereas on the western flank, at Mamsa, there is a decrease of about 0.50 m between the static water levels in May 2018 and December 2020 in the shallow aquifer, this can be attributed to low/reduced recharge, or exploitation. Thus, the current pumping practices in the aquifer on the western flank should be restrained for sustainable groundwater management. The analysis of the groundwater level fluctuations in this study is limited to the shallow hand-dug wells. We recommend that a long-term groundwater level monitoring in both shallow hand-dug wells and deep boreholes, together with spring discharge monitoring, be conducted in the study area. This will help water managers in Tanzania to make right decisions for the sustainable groundwater planning, utilisation, and management.

Funding

This research was funded by the Flemish Interuniversity Council-University Development Cooperation (VLIR-UOS) in the framework of project TZ2017TEA450A105 'Optimizing the valorization of water and rock resources for improved livelihoods in the Arusha volcanic region'.

CRediT authorship contribution statement

George Bennett: Conceptualisation, Data curation, Formal analysis, Investigation, Methodology, Resources, Software, Validation, Visualisation, Writing – original draft, Writing – review & editing. **Marc Van Camp**: Resources, Visualisation, Writing – review & editing. **Ceven Shemsanga**: Conceptualisation, Funding acquisition, Investigation, Methodology, Project administration, Resources, Supervision. **Matthieu Kervyn**: Conceptualisation, Funding acquisition, Project administration, Resources, Supervision. **Kristine Walraevens**: Conceptualisation, Investigation, Methodology, Resources, Supervision, Validation, Visualisation, Writing – review & editing.

Declaration of Competing Interest

The authors declare that they have no known competing financial interests or personal relationships that could have appeared to influence the work reported in this paper.

Data Availability

Data will be made available on request. The data presented in this study are available on request from the corresponding author.

Acknowledgments

The authors thank the Flemish Interuniversity Council - University Development Cooperation (VLIR-UOS) for funding this research. Also, the authors thank the Tanzania Commission for Science and Technology (COSTECH) for providing research permits. We also thank the two anonymous reviewers for their thoughtful comments that greatly improved this manuscript. Findings and conclusions in this paper are those of the authors and do not necessarily represent the official position of VLIR-UOS.

Institutional review board statement

Not applicable.

Informed consent statement

Not applicable.

Appendix

See appendix Tables 3–7.

Table 3
Manual groundwater level measurements on the northern flank of Ngurdoto crater.

Groundwater levels below ground surface (m)																			
Well ID	W1	W2	W3	W4	W5	W6	W6’	W13	W14	W15	W16	W17	W18	W19	W99	W7	W8	W9	W10
Date																			
05/07/2017	2.10	2.24	3.83					1.65	0.21	1.30	0.63	1.83	2.81	3.00					
15/07/2017	2.11	2.28	4.00	3.35		1.02		1.72	0.23	1.35	0.78	1.86	3.01	3.01		1.80	1.73	1.11	1.28
15/08/2018	1.32	1.75	3.32	0.58		0.65		2.10	1.65	1.25	1.05	1.55	4.15	1.68		1.60	1.21	2.08	1.60
19/09/2018	1.33	1.74	3.35	1.12	21.44	0.58		2.10	1.60	1.23	1.02	1.50	4.06	1.64		1.62	1.25	2.05	1.65
16/04/2019	3.34	3.74	5.34	3.52	21.25	0.54		2.50	0.32	1.35	2.95	2.65	4.80	1.80	0.20	4.38	3.77	1.10	0.56
20/05/2019	1.88	3.59	4.65	3.69	21.20	0.53		2.55	0.32	1.28	2.88	2.60	4.89	1.75	0.10	2.53	2.65	1.08	0.52
18/06/2019	1.68	2.45	4.48	3.13	21.15	0.51	0.37	2.50	0.29	1.25	0.77	2.54	2.92	1.56	0.00	2.42	2.32	1.13	0.40
18/07/2019	1.97	2.55	4.89	3.09	21.15	0.59	0.34	2.77	0.65	2.76	1.69	2.58	4.03	1.74	0.00	2.61	2.77	8.86	1.17
12/08/2019	2.27	2.71	5.05	3.17	21.04	0.54	0.34	3.15	1.35	2.37	3.13	3.10	4.48	1.86	0.00	2.72	2.80	6.74	2.20
09/09/2019	2.51	2.93	5.27	3.32	20.98	0.54	0.35	3.70	2.24	3.63	4.73	3.68	4.81	1.95	0.00	3.12	3.11	6.48	2.90
10/10/2019	2.30	3.17	5.49	3.55	20.92	0.37	0.30	4.12	3.00	4.33	5.06	4.17	4.75	1.88	0.00	2.40	3.14	6.80	3.69
07/11/2019	1.32	1.58	3.28	2.33	20.93	0.46	0.21	1.00	0.00	1.15	0.00	1.14	1.72	1.36	0.00	2.00	2.10	1.38	0.64
07/12/2019	1.12	1.75	3.49	2.00	20.83	0.37	0.14	0.56	0.00	0.53	0.00	1.14	2.13	1.48	0.00	1.95	2.01	1.48	0.26
17/04/2020	1.25	1.50	3.26	1.40	21.04	0.35	0.14	0.85	0.00	0.89	0.00	1.13	2.07	1.44	0.00	1.59	1.69	0.73	0.00
15/05/2020	1.08	1.22	3.25	0.00	21.00	0.33	0.00	0.98	0.00	0.92	0.00	1.30	2.14	0.85	0.00	0.00	0.12	0.45	0.00
15/06/2020	1.07	1.20	3.48	0.00	19.90	0.31	0.00	1.10	0.00	1.02	0.00	1.42	2.33	0.81	0.00	0.00	0.10	0.30	0.00
16/07/2020	1.18	1.57	3.87	0.00	19.88	0.22	0.00	1.52	0.00	1.40	0.21	1.97	3.22	0.98	0.00	0.42	0.30	0.69	0.00
10/08/2020	1.29	1.83	4.05	0.23	19.75	0.27	0.33	1.87	0.37	1.75	0.65	2.30	4.28	1.12	0.00	1.04	0.81	1.15	0.00
15/09/2020	1.72	2.14	4.52	0.75	19.69	0.30	0.36	2.47	1.53	3.37	2.38	2.93	4.42	1.17	0.00	1.64	1.24	4.46	0.28
21/10/2020	1.93	2.48	4.93	1.06	19.64	0.35	0.40	3.20	1.71	3.89	2.74	3.30	4.72	1.22	0.00	2.09	1.76	5.64	0.56
15/11/2020	2.15	2.60	5.25	1.24	19.50	0.37	0.41	3.80	4.42	4.10	3.87	3.94	4.97	1.30	0.00	2.32	2.05	5.83	1.68
29/12/2020	2.35	2.88	5.62	1.47	19.46	0.40	0.42	4.15	6.50	5.54	4.40	4.25	5.04	1.33	0.00	2.56	2.34	5.90	1.90

Table 4
Manual groundwater level measurements on the north-eastern flank of Mount Meru.

Groundwater levels below ground surface (m)									
Well ID	W11	W12	W24	W25	W70	W71	W91	W95	W96
Date									
12/07/2017	4.09	5.01	6.04						
04/09/2017	4.24	5.10	6.30		4.15	3.90			
16/09/2017	4.25	5.16	6.31		4.05	4.00			
24/09/2017	4.30	5.16	6.34		4.21	4.03			
17/04/2018	3.60	4.80	5.80	26.66	3.30	2.80			
03/05/2018	3.65	4.95	5.95	26.71	3.40	2.94			
25/05/2018	3.91	5.18	6.32	26.65	4.10	3.23			
08/06/2018	3.92	5.20	6.35	26.62	4.11	3.39	3.83		
21/06/2018	3.84	5.14	6.34	26.58	3.99	3.40	3.64		
20/07/2018	3.98	5.20	6.39	26.46	4.03	3.61	3.77		9.70
31/07/2018	3.98	5.20	6.37	26.41	4.01	3.48	3.73		9.70
17/09/2018	4.11	5.30	6.40	26.39	4.12	3.65	3.73	13.95	9.56
22/10/2018	4.32	5.32	6.15	26.36	4.05	3.88	3.78	13.95	9.59
27/11/2018	4.46	5.35	5.98	26.12	4.07	3.87	3.80	13.93	9.46
28/12/2018	4.46	5.35	6.25	26.11	4.21	3.96	3.80	13.91	9.44
27/01/2019	4.48	5.37	6.42	26.11	4.18	3.98	3.85	13.91	9.62
21/02/2019	4.48	5.38	6.47	26.09	4.01	3.94	3.73	13.90	9.70
04/03/2019	4.49	5.38	6.45	26.37	4.1	3.95	3.73	13.90	9.65
25/03/2019	4.50	5.39	6.46	26.23	4.03	4.03	3.75	13.91	9.66
08/04/2019	4.50	5.40	6.47	26.26	4.01	3.92	3.78	13.91	9.65
18/04/2019	4.50	5.40	6.50	26.22	4.06	3.94	3.82	13.92	9.67
24/04/2019	4.48	5.35	6.48	26.17	4.08	3.93	3.74	13.92	9.68
08/05/2019	4.47	5.29	6.40	26.14	3.93	3.77	3.63	13.90	9.60
20/05/2019	4.20	5.10	6.39	26.13	3.94	3.67	3.67	13.88	9.57
03/06/2019	4.15	5.09	6.39	26.12	3.95	3.67	3.72	13.88	9.55
17/06/2019	4.15	5.12	6.39	26.10	4.01	3.71	3.76	13.89	9.62
01/07/2019	4.23	5.14	6.38	25.98	4.02	3.81	3.78	13.88	9.57
18/07/2019	4.46	5.29	6.41	25.94	3.97	3.84	3.74	13.89	9.70
01/08/2019	4.48	5.29	6.40	25.95	3.97	3.86	3.66	13.89	9.60
12/08/2019	4.60	5.29	6.42	26.00	3.97	3.85	3.83	13.92	9.60
09/09/2019	4.60	5.32	6.44	26.04	3.95	3.88	3.69	13.89	9.60
10/10/2019	4.50	5.35	6.42	26.10	3.91	3.80	3.73	13.88	9.60
07/11/2019	4.45	5.30	6.39	26.07	3.88	3.74	3.66	13.87	9.57
07/12/2019	4.06	5.09	6.40	25.97	3.88	3.60	3.64	13.87	9.57
16/04/2020	3.78	4.99	6.29	25.70	3.93	3.28	3.61	13.83	9.47
15/05/2020	3.79	5.00	6.30	25.54	3.80	3.28	3.65	13.83	9.48
15/06/2020	3.80	5.10	6.32	25.26	3.75	3.30	3.72	13.82	9.50
16/07/2020	3.89	5.30	6.37	25.08	3.79	3.28	3.67	13.82	9.57
10/08/2020	3.95	5.32	6.36	24.99	3.85	3.31	3.71	13.81	9.56
15/09/2020	4.20	5.33	6.40	24.93	3.90	3.58	3.70	13.81	9.60
21/10/2020	4.29	5.35	6.43	24.86	3.93	3.72	3.70	13.80	9.63
15/11/2020	4.34	5.40	6.55	24.92	3.97	3.75	3.71	13.81	9.67
29/12/2020	4.35	5.41	6.77	25.06	3.98	3.78	3.71	13.82	9.69

Table 5
Manual groundwater level measurements on the western flank of Mount Meru.

Groundwater levels below ground surface (m)				
Well ID	W28	W28'	W29	W30
Date				
05/09/2017	47.35		38.11	45.60
16/09/2017	47.40		35.49	45.30
26/09/2017	47.45		35.77	45.30
03/05/2018	47.35		35.57	45.32
04/05/2018	47.35		35.57	45.32
25/05/2018	47.44		35.57	45.63
05/06/2018	47.68		35.58	45.63
09/06/2018	47.67		35.61	45.65
21/06/2018	47.68		35.84	45.63
20/07/2018	47.59		35.60	45.62
23/07/2018	47.60		35.63	45.64
06/08/2018	47.65		36.60	45.65
16/08/2018	47.60		36.73	45.65
17/09/2018	47.53		37.89	45.41
22/10/2018	47.66		35.65	45.65
27/11/2018	47.57		37.98	45.62
28/12/2018	47.49		37.69	45.85
27/01/2019	47.73		37.25	45.84
21/02/2019	47.68	47.24	35.74	45.90
22/02/2019	47.68	47.24	37.08	45.90
25/03/2019	47.75	47.27	35.76	47.78
08/04/2019	47.81	47.27	35.89	45.57
17/04/2019	47.81	47.23	35.77	45.57
24/04/2019	47.80	47.23	35.79	45.57
11/05/2019	47.63	47.22	35.79	45.56
20/05/2019	47.65	47.22	35.80	46.57
03/06/2019	47.63	47.23	35.81	46.22
17/06/2019	47.65	47.24	35.82	46.18
01/07/2019	47.81	47.27	35.97	45.59
19/07/2019	47.69	47.56	36.09	45.65
01/08/2019	47.70	47.29	36.00	46.14
13/08/2019	47.85	47.32	36.94	45.64
10/09/2019	47.80	48.26	35.88	45.99
10/10/2019	47.75	47.35	35.90	46.42
08/11/2019	47.75	47.36	35.92	45.70
08/12/2019	47.77	47.49	36.02	45.71
16/04/2020	47.82	47.48	35.98	45.76
15/05/2020	47.82	47.47	36.39	45.76
15/06/2020	47.85	47.46	36.01	45.78
16/07/2020	47.88	48.24	36.03	45.80
10/08/2020	47.90	47.49	36.02	45.80
15/09/2020	47.87	47.52	36.46	45.84
21/10/2020	47.90	47.65	36.07	45.86
15/11/2020	47.87	47.65	36.83	45.88
29/12/2020	47.88	47.64	36.67	45.89

Table 6
Manual groundwater level measurements on the south-western flank of Mount Meru.

Groundwater levels below ground surface (m)																	
Well ID	W31	W32	W33	W39	W42	W45	W46	W48	W51	W52	W55	W57	W58	W60	W62	W63	W64
Well depth (m)	22.8	15.8	14.4	17.1	17.8	30.6	15.7	16.7	24.2	41.0	11.6	16.5	12.9	14.6	7.7	9.0	12.4
Date																	
02/09/2017	17.89	13.80		15.06	15.95	28.16	14.93	14.71	21.37	39.60	5.94	14.90	11.28	12.43			9.03
04/05/2018	16.25	12.35		14.85	15.90	28.78	14.84	15.45	21.70	39.92	9.25	14.88	11.55	13.18			8.72
24/05/2018	17.01	12.09	10.44	14.75	15.72	28.76	14.72	15.38	21.62	39.90	9.20	14.87	11.50	13.15	5.80	6.82	8.69
05/06/2018	16.62	11.80	10.45	14.70	15.65	28.50	14.73	15.40	21.53	39.89	8.95	14.80	11.65	13.15	5.72	6.82	8.59
18/06/2018	15.87	11.51	10.73	14.68	15.50	28.12	14.70	14.79	21.49	39.88	8.82	14.75	11.76	12.45	5.60	6.80	8.60
03/07/2018	15.23	11.60	10.78	14.72	15.62	28.27	14.68	14.80	21.55	39.92	8.66	14.80	11.80	12.42	5.62	6.90	8.60
18/07/2018	14.97	11.25	10.87	14.68	15.30	28.22	14.67	14.74	21.04	39.87	8.64	14.57	11.13	11.71	5.90	7.05	8.62
02/08/2018	14.50	11.11	10.85	14.73	15.35	28.16	14.67	14.13	21.02	39.85	8.70	14.46	11.02	11.45	6.15	7.04	8.56
16/08/2018	14.37	11.10	10.80	14.72	15.32	28.18	14.65	14.10	21.00	39.82	8.82	14.34	10.60	11.39	6.25	7.05	8.56
22/09/2018	14.36	11.27	11.15	14.75	15.30	28.22	14.55	13.58	20.98	39.82	8.43	14.05	10.54	11.39	6.73	7.59	8.66
23/10/2018	14.59	11.49	11.25	14.74	15.32	28.24	14.49	13.50	20.88	39.85	8.34	14.05	10.26	11.92	6.75	7.49	8.60
28/11/2018	15.30	12.20	11.45	14.80	15.46	28.26	14.45	13.46	20.91	39.92	8.23	14.10	10.17	12.73	6.98	7.67	8.85
29/12/2018	16.20	13.10	11.60	14.86	15.54	28.28	14.44	13.47	20.91	40.00	8.63	14.15	10.37	13.33	7.01	7.01	9.25
28/01/2019	16.53	13.20	11.74	14.90	15.66	28.29	14.44	13.54	21.19	40.05	8.88	14.12	10.60	13.50	7.00	7.07	9.24
22/02/2019	16.31	13.25	11.87	14.92	15.70	28.30	14.45	14.78		40.05	8.90	14.18	10.03	13.72	7.31	7.75	9.20
06/03/2019	16.40	13.38	11.96	14.93	15.70	28.30	14.50	14.81		40.09	9.12	14.21	11.12	13.77	7.27	7.70	9.17
25/03/2019	17.15	13.60	12.05	14.93	15.79	28.86	14.48	15.00		40.24	9.21	14.52	11.36	13.94	7.26	7.80	9.37
19/04/2019	16.79	14.04	11.83	14.84	15.82	28.34	14.48	15.15		40.20	9.18	14.73	11.53	14.04	7.34	7.83	8.90
25/04/2019	16.93	15.08	12.49	14.88	15.91	28.51	14.50	15.39		40.26	9.33	15.10	11.70	14.15	7.36	7.85	9.21
11/05/2019	16.47	14.43	11.53	14.87	15.92	28.34	14.49	15.39		40.28	9.50	15.19	11.72	14.17	7.22	7.83	9.01
21/05/2019	16.45	14.25	11.35	14.84	15.88	28.33	14.49	15.36		40.30	9.34	15.24	11.73	14.15	7.11	7.73	8.91
04/06/2019	17.19	14.89	11.30	14.80	15.88	28.34	14.50	15.27		40.40	9.38	15.30	11.75	14.08	6.95	7.65	9.01
19/06/2019	16.86	15.00	11.59	14.76	15.92	28.43	14.51	15.21		40.46	9.83	15.33	11.79	13.97	6.85	7.57	8.74
02/07/2019	16.97	14.24	11.67	14.75	15.88	28.38	14.52	15.27		40.40	9.29	15.31	11.72	13.89	6.94	7.55	8.71
20/07/2019	16.87	14.15	11.70	16.46	15.84	28.80	14.53	15.33		40.47	9.56	15.36	11.84	13.80	7.11	7.72	8.89
02/08/2019	17.02	14.13	11.73	15.11	15.81	28.38	14.54	15.38		40.57	9.80	15.30	11.71	13.78	7.15	7.78	8.92
13/08/2019	17.21	15.23	11.75	15.55	15.72	28.37	14.55	15.47		40.57	9.65	15.32	11.72	13.81	7.25	7.79	9.62
10/09/2019	17.71	14.43	11.92	15.73	15.93	28.41	14.58	15.73		40.57	9.54	15.37	11.94	14.02	7.37	7.85	9.00
11/10/2019	17.69	14.47	11.68	14.90	16.06	29.02	14.60	15.88		40.56	9.46	15.47	11.84	14.21	7.36	7.88	9.06
08/11/2019	17.50	14.62	11.59	15.00	16.13	28.40	14.62	15.91		40.68	9.93	15.34	11.83	14.05	6.98	7.81	9.13
08/12/2019	16.72	14.09	11.39	15.65	16.00	28.38	14.63	15.72		40.73	9.27	15.27	11.71	13.69	6.85	7.84	8.96
18/04/2020	14.24	11.08	10.61	15.16	15.00	28.14	14.56	13.17		40.86	8.28	13.82	10.54	11.00	5.90	6.68	8.19
16/05/2020	13.60	10.73	10.58	14.65	14.85	27.98	14.47	12.38			8.02	13.35	10.02	10.40	5.22	6.47	8.05
16/06/2020	13.28	10.46	10.56	14.54	14.15	27.83	14.33	11.90			7.80	12.83	9.51	9.75	4.53	6.25	7.96
17/07/2020	13.15	10.39	10.63	14.41	14.00	27.77	14.03	11.67			7.65	12.50	9.09	9.57	4.98	6.54	7.95
11/08/2020	12.99	11.17	10.75	14.60	14.08	27.71	13.86	11.59			7.60	12.29	8.92	9.68	5.54	6.89	8.18
16/09/2020	13.15	10.73	10.80	14.67	14.15	27.75	13.77	11.63			7.65	12.21	8.70	10.24	6.12	7.10	8.70
22/10/2020	13.40	10.89	10.93	14.73	14.20	27.77	13.80	11.69			7.74	12.18	8.56	10.74	6.58	7.26	8.89
15/11/2020	13.60	11.10	10.93	14.60	14.24	27.77	13.83	11.83			7.95	12.58	8.63	11.38	6.68	7.47	8.30
30/12/2020	14.00	11.24	10.92	14.58	14.26	27.77	13.92	11.92			8.05	12.65	9.50	12.35	6.73	7.56	8.35

Groundwater levels below ground surface (m)

(continued on next page)

Table 6 (*continued*)

Well ID	W65	W66	W67	W69	W74	W75	W76	W77	W80	W82	W83	W85	W86	W87	W92	W93
Well depth (m	20.2	31.4	23.7	19.4	14.4	16.1	14.9	14.9	38.8	32.3	15.3	14.6	11.6	23.7	13.4	6.3
Date																
02/09/2017	19.30	30.07	23.25	14.00	9.41	14.48	12.93	11.63								
04/05/2018	18.65	30.05	22.60	12.75	9.60	14.67	13.65	12.40								
24/05/2018	18.62	30.00	22.50	12.60	9.58	14.64	13.60	12.36	33.48	28.95	13.38	3.98	7.62	22.10		
05/06/2018	18.48	29.80	22.50	12.40	9.58	14.62	12.77	12.25	33.23	28.85	13.38	3.98	7.62	22.10		
18/06/2018	18.45	30.00	22.50	12.38	9.57	14.54	12.71	12.20	32.97	31.10	12.72	4.89	7.61	22.09		
03/07/2018	18.52	30.00	22.50	12.40	9.51	14.60	12.52	12.28	33.15	30.13	12.70	4.97	7.78	22.12		
18/07/2018	18.27	29.90	22.45	12.84	9.39	14.21	12.10	11.25	32.87	29.80	11.98	5.06	8.09	22.05		4.09
02/08/2018	18.26	30.00	22.40	13.75	9.39	14.08	11.70	11.05	32.83	28.78	11.71	5.13	8.35	22.00		4.65
16/08/2018	18.25	30.00	22.40	14.40	9.39	13.76	11.75	11.80	32.76	28.78	11.45	5.20	8.65	22.05		4.70
22/09/2018	18.23	29.80	22.50	14.54	12.43	13.46	11.77	10.53	32.67	29.65	11.43	5.27	8.88	22.15		4.85
23/10/2018	18.19	29.80	22.60	14.67	9.26	13.16	11.77	10.42	32.71	29.67	11.43	5.23	8.96	21.74		4.85
28/11/2018	18.48	29.77	22.70	15.15	9.27	13.00	12.50	10.31	32.74	29.62	12.45	5.34	9.16	21.92		4.85
29/12/2018	18.64	29.80	22.80	15.86	9.40	13.09	13.75	10.47	32.79	28.79	13.98	5.30	9.40	21.83		4.80
28/01/2019	18.67	29.80	22.90	15.44	9.23	13.39	14.20	10.87	32.95	28.78	13.53	5.30	9.28	22.18		4.80
22/02/2019	18.63	29.90	22.90	16.05	9.36	13.86	14.84	11.20	32.90	28.80	13.76	5.44	9.50	23.63		4.94
06/03/2019	18.59	29.90	22.80	16.07	9.40	13.96	14.88	12.03	32.90	28.80	13.84	5.45	9.52	22.70		4.95
25/03/2019	18.66	30.00	22.90	16.18	9.41	14.26	14.52	12.29	33.13	28.94	13.94	5.55	9.60	22.90		5.05
19/04/2019	18.73	30.00	22.80	16.28	9.86	14.67	14.64	12.48	33.65	28.91	14.04	5.60	9.69	23.10		4.99
25/04/2019	18.8	30.00	22.90	16.43	9.40	14.68	14.75	12.70	33.16	28.95	14.13	5.62	9.74	23.50	12.61	5.10
11/05/2019	18.81	30.00	22.90	16.48	9.41	14.93	14.86	12.75	33.10	30.11	14.14	5.54	9.62	23.50	12.62	4.98
21/05/2019	18.83	30.00	22.80	16.50	9.44	14.96	14.88	12.79	33.15	28.84	14.17	5.33	9.35	23.63	12.62	4.85
04/06/2019	18.78	30.00	22.80	16.46	11.98	15.13	14.67	12.82	33.18	28.90	14.08	5.23	8.94		12.56	4.77
19/06/2019	18.71	30.10	22.80	16.47	9.45	14.98	14.53	12.74	33.27	28.98	14.00	5.28	8.95		12.53	4.78
02/07/2019	18.65	30.00	22.80	16.49	10.57	14.96	14.40	12.69	33.21	29.27	13.92	5.24	8.95		12.51	4.80
20/07/2019	18.61	30.20	22.80	16.51	9.45	14.94	14.31	12.62	33.70	29.30	13.86	5.35	9.06		12.52	4.96
02/08/2019	18.61	30.20	22.80	16.51	10.04	14.94	14.28	12.70	33.41	29.10	13.89	5.37	9.25		12.54	4.98
13/08/2019	18.65	30.30	22.80	16.53	9.61	15.22	14.37	12.81	33.23	31.48	13.91	5.36	9.45		12.58	4.96
10/09/2019	18.82	30.30	22.90	16.56	9.43	15.25	14.61	13.86	33.37	29.22	14.65	5.77	9.67		12.65	5.04
11/10/2019	18.96	30.30	22.90	16.72	9.30	15.08	14.84	12.98	33.86	29.29	14.25	5.75	9.81		12.67	5.05
08/11/2019	18.98	30.40	22.90	15.82	9.34	15.10	14.62	13.19	33.18	31.13	14.07	4.85	9.16		12.60	4.74
08/12/2019	18.96	30.40	22.80	15.41	9.41	14.92	14.13	12.80	33.18	29.29	13.63	4.88	8.63		12.49	4.45
18/04/2020	17.93		21.30	11.82	9.46	13.31	11.17	11.26	33.50	28.57	10.23	4.89	7.70		11.20	3.17
16/05/2020	17.62		21.60	11.50	9.22	12.75	10.52	10.31	32.69	28.38	9.86	4.85	7.42		10.52	2.83
16/06/2020	17.31		21.80	11.20	8.96	12.27	9.90	9.41	33.08	28.26	9.66	4.81	7.20		9.98	2.65
17/07/2020	17.12		21.80	11.66	8.98	11.82	9.69	9.03	32.43	28.07	9.42	4.88	7.66		9.74	2.36
11/08/2020	16.82		21.80	12.17	9.02	11.57	9.84	8.88	32.55	28.38	9.53	4.98	7.97		9.79	2.85
16/09/2020	16.98		22.10	13.15	9.03	11.33	10.47	9.10	32.28	28.21	10.13	5.16	8.41		10.23	3.30
22/10/2020	17.07		22.10	14.03	9.05	11.38	11.00	9.18	33.29	28.10	10.62	5.27	8.76		10.64	3.71
15/11/2020	17.28		22.20	14.18	9.31	11.50	12.32	9.83	32.10	28.10	11.38	5.30	8.87		11.25	3.95
30/12/2020	17.33		22.30	14.23	8.47	11.99	12.78	10.15	32.08	28.00	12.20	5.33	8.98		11.93	4.02

Table 7
Extra manual groundwater level measurements on the flanks of Mount Meru.

Region	Well ID	Elevation (m)	Well Depth (m)	Water Depth (m)	Date	Water Depth (m)	Date	Water Depth (m)	Date	Water Depth (m)	Date	Water depth (m)	Date
Nkoasenga and Leguruki	W20	1348	5.0	2.66	11/07/2017	2.72	19/07/2017						
	W21	1441	50.0	38.00	09/07/2017								
Mkuru and Ngarenanyuki	BH11	1544	64.5	29.88	20/01/2008								
	BH26	1551	47.5	38.19	16/04/2019								
	W81	1371	21.0	20.00	17/04/2018								
	W102	1553	38.5	37.36	21/10/2020	36.35	22/10/2020						
Mamsa	W89	1647	41.5	40.30	25/05/2018								
Ngaramtoni and Arusha town	BH13	1476	129.0	33.67	25/03/2018								
	BH14	1479	150.0	43.51	26/03/2018								
	BH15	1595	115.0	33.00	13/02/2013								
	BH 17/2002	1496	81.0	45.80	04/03/2019								
	BH 157/2011	1531	77.0	72.16	04/04/2019								
	W35	1561	50.0	14.82	24/05/2018	15.44	18/06/2018	15.48	02/07/2018	16.16	18/07/2018	16.90	22/09/2018
	W36	1561	19.1	14.78	24/05/2018	15.19	18/06/2018	15.25	02/07/2018	16.76	22/09/2018	14.32	23/10/2018
	W40	1576	28.9	28.43	02/09/2017	27.42	24/05/2018	26.77	18/06/2018	26.70	18/07/2018	26.64	22/09/2018
	W41	1574	23.9	22.38	02/09/2017	22.12	19/06/2018	22.25	02/07/2018				
	W43	1513	29.8	27.60	03/09/2017	27.23	21/05/2018	27.30	03/07/2018	26.81	22/09/2018	26.68	06/03/2019
	W44	1511	30.1	28.71	03/09/2017	29.15	23/09/2017	29.16	22/05/2018				

(*continued on next page*)

Table 7 (*continued*)

Region	Well ID	Elevation (m)	Well Depth (m)	Water Depth (m)	Date	Water Depth (m)	Date	Water Depth (m)	Date	Water Depth (m)	Date	Water depth (m)	Date
	W49	1559	23.0	19.80	03/09/2017	19.95	23/09/2017						
	W53	1572	16.5	12.90	03/09/2017	12.77	19/06/2018	12.79	04/07/2018	12.83	22/09/2018	12.96	06/03/2019
	W56	1523	12.9	11.20	10/09/2017	11.28	23/05/2018	11.29	20/06/2018	11.28	04/07/2018		
	W59	1547	17.0	14.60	10/09/2017								
	W68	1577	18.0	15.43	02/09/2017	15.78	26/09/2017						
	W79	1537	18.2	16.21	13/09/2017	16.32	24/05/2018	15.60	18/06/2018	15.72	03/07/2018		
	W84	1546	15.8	13.89	23/05/2018	13.42	20/06/2018	12.92	01/08/2018	12.49	23/09/2018		
	W90	1529	17.8	15.70	06/06/2018	15.66	19/06/2018	15.68	03/07/2018	15.60	02/08/2018	14.73	22/09/2018
	W94	1575	8.2	6.96	18/07/2018								
	W97	1526	20.0	19.70	03/06/2019								
	W100	1385	8.9	6.36	14/08/2019								
	W101	1373	2.3	1.63	14/08/2019								

References

Mapsland, 2021. Large topographical map of Tanzania. Accessed 16–07-2021 from ⟨https://www.mapsland.com/africa/tanzania/large-topographical-map-of-tanzania⟩.

Bennett, G., Van Reybrouck, J., Shemsanga, C., Kisaka, M., Tomašek, I., Fontijn, K., Kervyn, M., Walraevens, K., 2021. Hydrochemical characterisation of high-fluoride groundwater and development of a conceptual groundwater flow model using a combined hydrogeological and hydrochemical approach on an active volcano: Mount Meru, Northern Tanzania. Water 13 (16), 2159. https://doi.org/10.3390/w13162159.

Bennett, G., Van Reybrouck, J., Shemsanga, C., Kisaka, M., Tomašek, I., Fontijn, K., Kervyn, M., Walraevens, K., 2022a. Identification of low fluoride areas using conceptual groundwater flow model and hydrogeochemical system analysis in the aquifer system on the flanks of an active volcano: Mount Meru, Northern Tanzania. Sci. Total Environ. 814 (C), 152682 https://doi.org/10.1016/j.scitotenv.2021.152682.

Bennett, G., Shemsanga, C., Marc Van Camp, Kervyn, M., Walraevens, K., 2022b. Delineation of the aquifer structure and estimation of hydraulic properties on the flanks of Mount Meru, Northern Tanzania. J. Afr. Earth Sci. 196C, 104673 https://doi.org/10.1016/j.jafrearsci.2022.104673.

Cui, Y., Liao, Z., Wei, Y., Xu, X., Song, Y., Liu, H., 2020. The response of groundwater level to climate change and human activities in Baotou city, China. Water 12 (4), 1078. https://doi.org/10.3390/w12041078.

Ghiglieri, G., Balia, R., Oggiano, G., Pittalis, D., 2010. Prospecting for safe (low fluoride) groundwater in the Eastern African Rift: the Arumeru District (Northern Tanzania). Hydrol. Earth Syst. Sci. 14 (6), 1081–1091. https://doi.org/10.5194/hess-14-1081-2010.

Healy, R.W., Cook, P.G., 2002. Using groundwater levels to estimate recharge. Hydrogeol. J. 10, 91–109. https://doi.org/10.1007/s10040-001-0178-0.

Kong, F., Xu, W., Mao, R., Liang, D., 2022. Dynamic changes in groundwater level under climate changes in the Gnangara region, western Australia. Water 14 (2), 162. https://doi.org/10.3390/w14020162.

Lee, J.M., Woo, N.C., Koh, D.-C., Kim, K.-Y., Ko, K.-S., 2020. Assessing aquifer responses to earthquakes using temporal variations in groundwater monitoring data in alluvial and sedimentary bedrock aquifers. Geomat., Nat. Hazards Risk 11 (1), 742–765. https://doi.org/10.1080/19475705.2020.1751310.

Maréchal, J.C., Sarma, M.P., Ahmed, S., Lachassagne, P., 2002. Establishment of earth tide effect on water-level fluctuations in an unconfined hard rock aquifer using spectral analysis. Curr. Sci. 83 (1), 61–64.

Marques, E.A.G., Silva Junior, G.C., Eger, G.Z.S., Ilambwetsi, A.M., Raphael, P., Generoso, T.N., Oliveira, J., Júnior, J.N., 2020. Analysis of groundwater and river stage fluctuations and their relationship with water use and climate variation effects on Alto Grande watershed, Northeastern Brazil. J. South Am. Earth Sci. 103, 102723 https://doi.org/10.1016/j.jsames.2020.102723.

Shibata, T., Takahashi, R., Takahashi, H., Kagoshima, T., Takahata, N., Sano, Y., Pinti, D.L., 2020. Coseismic changes in groundwater level during the 2018 Hokkaido Eastern Iburi earthquake. Earth, Planets Space 72, 23. https://doi.org/10.1186/s40623-020-01152-y.

Singaraja, C., Chidambaram, S., Jacob, N., 2018. A study on the influence of tides on the water table conditions of the shallow coastal aquifers. Appl. Water Sci. 8, 11. https://doi.org/10.1007/s13201-018-0654-5.